Department of Astronomy

Faculty of Science

University of Helsinki, Finland

# Two views on interstellar dust: near-infrared scattering and polarized thermal dust emission

Veli-Matti Pelkonen

ACADEMIC DISSERTATION

*To be presented, with the permission of the Faculty of Science of the University of Helsinki, for public criticism in Auditorium XIV of the University Main Building on Friday, 2nd of October 2009, at 12 o'clock noon.*

**Cover, left:** A part of a filament in Corona Australis Molecular cloud. The image is a composite of $J$-, $H$-, and $Ks$-band (coded blue, green, and red) near-infrared observations made in August 2006 using NTT/SOFI at La Silla, Chile. The surface brightness is due to near-infrared scattered light and is a tracer of the dust column density. The change in color is due to saturation of shorter wavelengths in larger extinctions. The center of the filament is seen as a darker, starless spot, where all three wavelengths are saturated. The data was analyzed in Paper III. (ESO Press Photo 06/08, 7th of March 2008)

**Cover, right:** Two simulated polarization maps. The background color is the logarithm of intensity of thermal dust emission in MJy/sr at 353 GHz, and the polarization vectors are plotted in white. The upper frame shows alignment calculated from a constant anisotropy factor (Paper V), whereas in the lower frame the anisotropic radiation field is calculated for each computational cell (Paper VI). A version of this picture appeared first in Paper VI, and was selected as a cover picture for that issue of *Astronomy & Astrophysics*.

# Abstract

Interstellar clouds are not featureless, but show quite complex internal structures of filaments and clumps when observed with high enough resolution. These structures have been generated by

1) turbulent motions driven mainly by supernovae,

2) magnetic fields working on the ions and, through neutral-ion collisions, on neutral gas as well, and

3) self-gravity pulling a dense clump together to form a new star.

The study of the cloud structure gives us information on the relative importance of each of these mechanisms, and helps us to gain a better understanding of the details of the star formation process.

This thesis is concerned with the interstellar dust. Interstellar dust is often used as a tracer for the interstellar gas which forms the bulk of the interstellar matter. Some of the methods that are used to derive the column density are summarized in this thesis. In particular, a new method, which uses the scattered light to map the column density in large fields with high spatial resolution, is introduced. In addition to the density structure, this thesis also takes a look at the grain alignment with respect to the magnetic fields. The aligned grains give rise to the polarization of starlight and dust emission, thus revealing the magnetic field. The alignment mechanisms have been debated for the last half century. The strongest candidate at present is the radiative torques mechanism, which is the other main topic of this thesis.

In the first four papers included in this thesis, the scattered light method of column density estimation is formulated, tested in simulations, and finally used to obtain a column density map from observations. They demonstrate that the scattered light method is a very useful and reliable tool in column density estimation, and is able to provide higher resolution than the near-infrared color excess method. These two methods are complementary. The derived column density maps are also used to gain information on the dust emissivity within the observed cloud.

The two final papers present simulations of polarized thermal dust emission assuming that the alignment happens by the radiative torques mechanism. We show that the radiative torques can explain the observed decline of the polarization degree towards dense cores. Furthermore, the results indicate that the dense cores themselves might not contribute significantly to the polarized signal, and hence one needs to be careful when interpreting the observations and deriving the magnetic field.

# Acknowledgements

This thesis would not exist had it not been for the opportunities and the guidance offered to me by Mika Juvela. It has been a joy and a privilege to work with him and to learn from him. I hope to have the pleasure of continuing to collaborate with him in the future as well even though I am no longer his student. Although I certainly have a lot to learn from him still! So thanks, Mika, for everything. You are an example to aspire to.

I would be remiss if I did not offer thanks to the rest of the Astronomy Department up at Tähtitorninmäki, too. Wonderful people who offered many stimulating discussions whether it was on the current topics of astronomy, problems of data reduction or 'funny' results, university administration, or just about home cooking. Great people to work with. I especially would like to single out Professor Kalevi Mattila, whose warm and knowledgeable leadership of the Interstellar Medium group fostered a real sense of family within the group. From the start in the spring of 2005, I felt like being part of a great team, and my respect for him both as a man and as an astronomer has just grown as I have come to know him better. For his help and advice in preparing for my thesis examination I am truly grateful.

There are many important women in my life who deserve a mention. Michele, you know how important you are to me, and I probably do not tell you that often enough. Thank you for being there for me. Suvi and Niina, two of my sisters. I hope I have done well by both of you as a little brother and a big brother, respectively. Thank you, Suvi, for suffering my company these years, and thank you, Niina, for all the cheerful hugs and laughs we have shared. And of course my Mother, Hillevi, whose unconditional love and support is something any son would be proud to have. I am also glad to have two more fine siblings from my father's side, Jani and Saija. Pity we have not had more time together. My father, Alpo, has been and still is an example for me what a man should be like.

I have been blessed with a cadre of good friends, without whom life would certainly have been a lot duller and stressful. So let me just try to acknowledge some of you here: Hanna S., Juha, Pertti, Matias and Salli, Kimmo and Anna, Antti, Leena, Hanna L., Pauli, Ville, Harri, Jari, Juliet, Pip and Tull. To all of my friends, named and unnamed, thanks for your friendship and for making life fun.

# List of publications

**I**    Padoan P., Juvela M., & **Pelkonen V.-M.**, 2006, "High-resolution mapping of interstellar clouds by near-infrared scattering", *The Astrophysical Journal Letters*, 636, L101

**II**    Juvela M., **Pelkonen V.-M.**, Padoan P., & Mattila, K., 2006, "High-resolution mapping of interstellar clouds by near-infrared scattered light", *Astronomy & Astrophysics*, 457, 877

**III**    Juvela M., **Pelkonen V.-M.**, Padoan P., & Mattila K., 2008, "A Corona Australis cloud filament seen in NIR scattered light. I. Comparison with extinction of background stars", *Astronomy & Astrophysics*, 480, 445

**IV**    Juvela M., **Pelkonen V.-M.**, & Porceddu S., "A Corona Australis cloud filament seen in NIR scattered light. II. Comparison of infrared and sub-millimeter data", accepted to *Astronomy & Astrophysics* on 21th of July, 2009 (arXiv:0907.4633v1 [astro-ph.GA])

**V**    **Pelkonen V.-M.**, Juvela M., & Padoan P., 2007, "Simulations of polarized dust emission", *Astronomy & Astrophysics*, 461, 551

**VI**    **Pelkonen V.-M.**, Juvela M., & Padoan P., "Predictions of polarized dust emission from interstellar clouds: spatial variations in the efficiency of radiative torque alignment", *Astronomy & Astrophysics*, 502, 833

# Contents

# Chapter 1

# Interstellar medium

The space between the stars is filled by extremely low density medium, the so-called interstellar medium (ISM), which consists of ordinary matter (gas and dust) and relativistic charged particles known as cosmic rays. While the ISM corresponds to only a small fraction of the visible mass of the Galaxy, around 10% - 15%, it is a vital part of the physical and chemical processes that take place in the Galaxy.

## 1.1   History

In the late eighteenth century, the famous astronomer William Herschel noticed that some patches on the night sky, especially towards the Milky Way, were empty of stars. The first long exposure photographs of the Milky Way by e.g. Edward Barnard showed many more dark zones (Barnard, 1927). Soon it was realized that these apparent holes were due to dark clouds of interstellar matter blocking the light of stars behind them. Trumpler (1930) showed that even the apparently transparent interstellar space was actually occupied by dust, which dimmed and caused the stars to appear redder the farther away they were.

The more diffuse clouds had been suspected to exist ever since the discovery of stationary absorption lines of CaII in the spectrum of a binary star $\sigma$ Orionis by Hartmann (1904). The spectral lines of the two stars underwent periodic changes due to the Doppler shifts caused by their orbital motion, but the CaII-line stayed stationary. Hence, it must have arisen in interstellar space along the line of sight, not in the binary stars. Later, more stationary lines were detected in the spectra of other stars, revealing the presence of several clouds of differing velocity on the line of sight (e.g. Beals, 1936; Adams, 1949).

The existence of interstellar magnetic field was postulated by Davis & Greenstein (1951), when they proposed that the linear polarization of starlight detected a couple of years earlier (Hall, 1949; Hiltner, 1949) could be explained if param-

agnetic, non-spherical, rapidly spinning grains would align themselves according to the magnetic field. Davis & Greenstein used this theory to map the local interstellar magnetic field and found that it is tangentially oriented to the Galactic disk.

Cosmic rays were first proven to be of extraterrestrial origins by a balloon experiment by Hess (1919). It took another decade until they were discovered to be highly energetic charged particles rather than photons (Bothe & Kohlhörster, 1929), but the name stuck. Ginzburg & Syrovatskii (1965) identified the observed Galactic radio emission with synchrotron radiation by cosmic-ray electrons gyrating around magnetic field lines, which meant that the cosmic rays were widespread in the Galaxy. The composition of the cosmic rays is predominately protons, with $\sim 10\%$ helium nuclei, $\sim 1\%$ heavier nuclei, $\sim 2\%$ electrons, and smaller amounts of positrons and antiprotons (Blandford & Eichler, 1987; Bloemen, 1987). While the majority of the low-energy cosmic rays originate from the Sun, the more energetic ones originate outside the solar system.

## 1.2   ISM-star cycle

The ISM-star cycle is important, because almost all of the elements heavier than hydrogen and helium, are formed inside the stars. Our Sun is a second generation star, formed from enriched ISM. Terrestrial planets, the oxygen and nitrogen in the Earth's atmosphere, the carbon that is the basic building block for life on Earth, all come from the interiors of long-dead stars.

The matter of the ISM is not uniformly distributed across interstellar space, but shows dramatic differences in both density and temperature. Only the coldest, densest molecular regions are suitable for star formation. In these sites, small clouds of interstellar gas tend to become gravitationally unstable and collapse to form new stars, if the magnetic pressure, the gas pressure and the turbulent motions are unable to counteract this. The contraction of a prestellar core, once it starts to collapse, is swift, taking less than a million years.

Once the star has formed, the accreted matter is mostly trapped inside it by gravity. Within the interiors of the stars, thermonuclear fusion takes place that enriches the matter in heavy elements. Both the lifespan of a star and the elements that it eventually produces depend on the mass of the star. The more massive the star is, the faster it burns out and the heavier are the elements that it produces. The massive stars, over 8 solar masses, shine as brightly as thousands of Suns, but live only some tens of millions of years. Sun is considered to be an average star, and its lifespan is about ten billion years. The smallest stars, with masses less than one tenth of solar mass, are expected to last hundreds of billions

of years.

Some of the matter eventually returns to the ISM through continuous stellar winds, through mass-ejections in the red giant phase of medium-mass stars, or through an instantaneous and violent supernova explosion, either a core-collapse supernova in a massive star or a thermonuclear one in a binary system. All these methods inject energy into the ISM along with the enriched matter, which does not only power turbulent motions, but also contributes to the heating of the ISM and stirs it, maintaining the heterogeneous structure of the ISM. Under the right circumstances, these motions caused by one star can disturb the balance of another region of cold molecular matter, causing new stars to form from the collapsing clouds, restarting the ISM-star cycle.

## 1.3  Composition

The matter of the ISM is roughly 90% hydrogen and 10% helium by number, with trace amounts of heavier elements. A significant amount of the heavier elements ('metals', in common parlance of astronomers) is missing from the gaseous phase, having formed dust grains, although the exact amount varies. Measured by its mass, the interstellar dust makes up 0.5 - 1 % of the interstellar matter in the present day Galaxy, but since it is coupled with the gaseous phase, it is an important tracer for the gas and thus the mass of the interstellar matter. In the following, the different forms of the interstellar gas are described, while dust is discussed in the next chapter.

### 1.3.1  Hot ionized gas

Spitzer (1956) postulated the presence of a Galactic corona, made of rarefied, hot interstellar gas, which would provide the necessary pressure to confine the high latitude interstellar clouds. Two decades later, the *Copernicus* satellite detected broad UV absorption lines of high-stage ions, which only form at elevated temperatures, in the spectrum of several bright stars (Jenkins & Meloy, 1974; York, 1974). From O VI (five-times-ionized oxygen) and N V (four-times-ionized nitrogen) lines it was possible to deduce that the necessary temperature was a few times $10^5$ K (York, 1974, 1977). Around the same time, Williamson et al. (1974) suggested that the soft X-ray background radiation was probably due to thermal emission from hot interstellar plasma, about $10^6$ K in temperature (McCammon and Sanders, 1990). Later observations revealed even hotter superbubbles of hot gas, reaching temperatures up to a few $10^6$ K (Aschenbach, 1988; McCammon and Sanders, 1990). Using the all sky survey of the *ROSAT* satellite, Snowden et al. (1998) derived a hydrogen density $\simeq 0.0065 \mathrm{cm}^{-3}$ for the hot gas in the
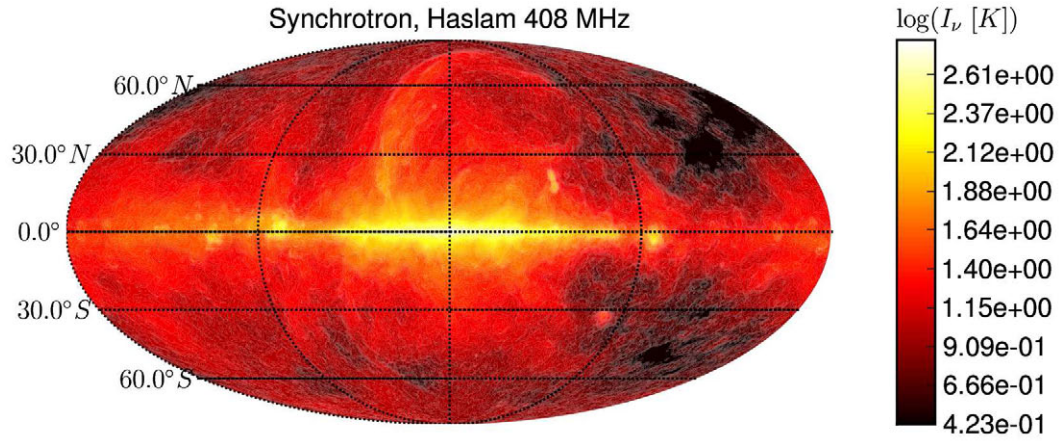
Figure 1.1: Haslam 408 MHz map showing the synchrotron radiation of the hot ionized gas. (Haslam et al., 1982; LAMBDA archive, NASA Office of Space Science)

Local Bubble.

Hot interstellar gas is generated mainly by supernova explosions, and, to a lesser extent, by powerful stellar winds from O and B stars (e.g. McCray & Snow, 1979; Spitzer, 1990). Supernova shock waves traveling through the ISM heat the gas and hollow out cavities of rarefied, hot gas, surrounded by a cold dense shell of interstellar matter. Cox & Smith (1974) noted that the hot gas inside the cavities will last for millions of years due to their long radiative cooling times, and thus might join up with another supernova bubble into a network. The presence of the interstellar magnetic pressure substantially reduces the filling factor of the hot gas (Slavin & Cox, 1993; see also McKee, 1990). Since core-collapse supernovae occur mainly in young clusters of stars, the result is often superbubbles rather than individual supernova remnants (McCray & Snow, 1979; Heiles, 1987).

### 1.3.2 Warm ionized gas

The hottest and most massive stars in the Galaxy emit intensely in the UV wavelength. When the wavelength is below 912 Å, UV radiation is able to ionize hydrogen atoms. Therefore, O and B stars are surrounded by an ionized H II region, which ends abruptly to a neutral H I boundary. The radius of this boundary around the star is called the Strömgren radius. Inside the shell, the hydrogen ions recombine with free electrons before being ionized by the UV radiation of the star once more. Beyond Strömgren radius, the recombination rate is larger than the photoionization rate. A fraction of the photoionizing radiation goes to heating the interstellar gas. Balancing the radiative cooling of

the gas and the photoelectric heating, the equilibrium temperature is $\simeq 8000$ K (Mallik, 1975; Osterbrock, 1989). This is well in accordance with the observations (Osterbrock, 1989; Reynolds, 1985). H II regions radiate in radio continuum due to "free-free" emission generated by the free electrons accelerated in the electric field of the positive ions. They also radiate in emission lines by the de-excitation of atoms, which have been excited by recombination (hydrogen, helium) or by collisions (metals). Of particular interest is the H$\alpha$ emission line that arises from the transition of an electron from level n=3 to n=2, producing a photon at 6563 Å.

Struve & Elvey (1938) detected H$\alpha$ emission from extended zones in Cygnus and Cepheus, outside the well-defined H II regions. Later studies of H$\alpha$ photographic surveys (e.g. Sivan, 1974) and H$\alpha$ spectroscopic scans (e.g. Roesler et al., 1978) showed that diffuse H$\alpha$-emitting gas exists in all directions in the sky. The Wisconsin H$\alpha$ Mapper (WHAM) survey (Haffner et al., 2003) mapped the distribution and kinematics of the H$\alpha$-emitting gas over the northern sky above $-30$ deg in declination, confirming that the warm ionized gas was ubiquitous in the Milky Way.

There is still some debate as to how these extended H$\alpha$-emitting regions form. O stars are capable of ionizing their surroundings, but they are born in dense molecular clouds, where it is difficult for the ionizing photons to escape to ionize the observed high-latitude warm ionized gas (Reynolds, 1984). This might be explained by some of the nearby O stars being powerful enough to cause their H II regions to grow up to observed high latitudes (Miller & Cox, 1993). Dove & Shull (1994) suggested that superbubbles formed by OB associations would provide natural cavities for the ionizing radiation to escape to high latitudes (see also Dove et al., 2000). The observed line-emission spectrum of the warm ionized regions differs from the characteristic spectrum of a H II region around an O star (Reynolds, 1985), and varies spatially on the sky. The former might be explained by the addition of weak-shock excitation (Sivan et al., 1986) or a very dilute ionizing radiation field from a plausible mixture of O stars (Mathis, 1986; Domgörgen & Mathis, 1994). The spatial variations of the emission line ratios seem to require additional ionization/heating sources to explain them (Reynolds et al., 1999).

### 1.3.3 Neutral atomic gas

Neutral atomic hydrogen, H I, can be observed in the interstellar 21-cm line emission, first proposed by van de Hulst (1945) and pioneered by Ewen & Purcell (1951). 21-cm line emission is generated by the flipping of the magnetic spin of the electron from parallel to the spin of the nucleus to antiparallel. The
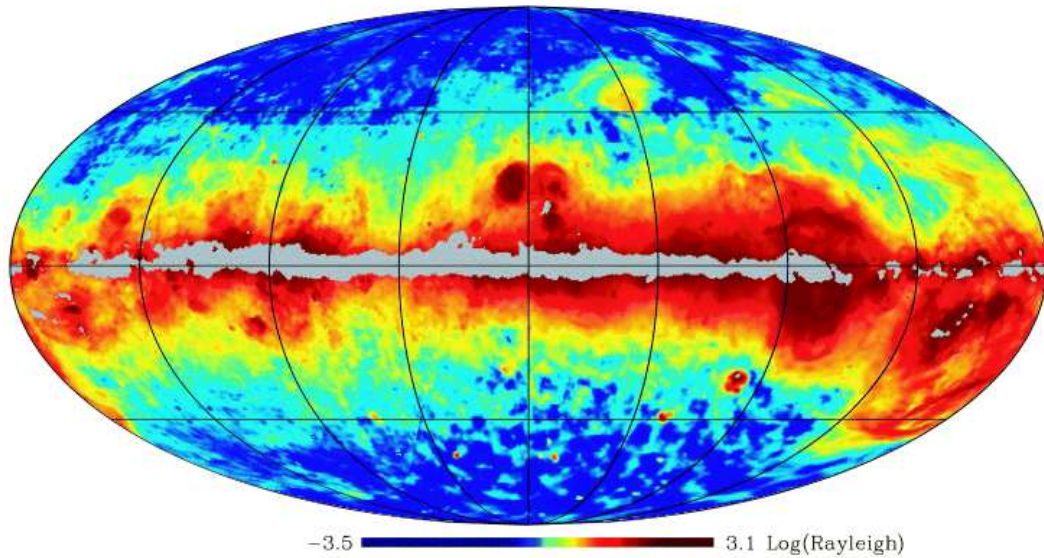
Figure 1.2:   Extinction-corrected Hα emission map by Dickinson et al. (2003). Areas of extinction larger than 1 magnitude have been masked in grey, since the true Hα extinction is uncertain.

21-cm radiation penetrates the interstellar matter easily and thus gives the total H I column density in the observed direction. The observed 21-cm spectra show superimposed line emissions at different Doppler shifts. This allows for the separation of the distinct line profiles into H I clouds orbiting the Galactic center at different distances and hence at different velocities. H I maps projected onto the plane of the Galaxy show a spiral structure (Oort et al., 1958; Mihalas & Binney, 1981), revealing the spiral arms of the Milky Way. According to Kulkarni et al. (1982), the surface density of H I in spiral arms is four times that of the interarm regions. While H I does not emit in the optical, the Lyman $\alpha$ (L$\alpha$) transition of an electron from ground state n=1 to excited state n=2 causes an absorption line at 1216 Å in the UV. This line has been used since late 1960s and early 1970s to study the local ISM (Morton, 1967; Savage & Jenkins, 1972; Jenkins & Savage, 1974), but due to the absorption of UV photons by the interstellar matter, it is unable to penetrate deeply to the ISM.

The broad emission lines of 21-cm reveal the presence of warm neutral gas of temperature $\simeq 6000 - 10000$ K (Dickley et al., 1978; Kulkarni & Heiles, 1987). Field et al. (1969) predicted theoretically that there should be two H I phases of comparable thermal pressures but different densities and temperatures (see also Goldsmith et al. 1969). The cold, dense phase is cooled by radiation of the collisionally excited fine-structure lines of metals, while the rarefied, warm phase is cooled by the onset of L$\alpha$ cooling at 8000 K. The cold H I shows up in narrow

absorption lines in the 21-cm spectrum, with the estimated temperature of 50 - 100 K. The cool H I gas is about hundred times as dense as the warm, diffuse intercloud H I, $n = 20 - 50 \text{cm}^{-3}$ compared to $n = 0.2 - 0.5 \text{cm}^{-3}$ (Kulkarni & Heiles, 1987).

### 1.3.4 Molecular gas

Interstellar molecular absorption lines were observed in the optical spectra of stars in the 1930s (e.g. Merrill, 1934; Russell, 1935; Swings & Rosenfeld, 1937). However, only in the 1970s was it possible to do UV astronomy above the Earth's atmosphere to detect the most common interstellar molecule, molecular hydrogen $H_2$, in the far-UV spectrum of a hot star (Carruthers, 1970). The second-most abundant molecule, CO, was found by Smith & Stecher (1971), also in a UV stellar spectrum. However, UV radiation of stars is able to penetrate only the more tenuous outer layers of the molecular clouds, due to the strong interstellar extinction. To probe the interiors of the molecular clouds and the clouds located farther away, radioastronomy is the key.

$H_2$ unfortunately is not observable in radio wavelengths, and thus astronomers use CO as a tracer of $H_2$ (e.g. Scoville & Saunders, 1987). The CO molecule has a rotational transition at 2.6 mm, and the corresponding emission line was actually found a couple of months before the detection of CO in UV (Wilson et al. 1970). The Galactic rotation curve can be used to place the superposed CO spectral features on the correct Galactocentric distances, as in the case of neutral atomic gas. Dame et al. (2001) provide composite of CO surveys of H I lines covering the entire Galactic disk. There is a distinct molecular ring at $\simeq 4.5$ kpc from the Galactic center, and the molecular clouds seem to follow the spiral arm distribution (Clemens et al., 1988). Interarm regions are not empty, but the amount of molecular gas is lower by a factor of $\sim 3.6$ within the solar distance from the center (Clemens et al., 1988), and much lower in the outer Galactic disk, by a factor of 13 (Grabelsky et al., 1987; Heyer, 1999). Molecular gas is strongly concentrated to the Galactic plane, with scale height less than 100 pc (Clemens et al., 1988).

High-resolution observations (e.g. Heyer et al., 1998) indicate that the molecular gas is in discrete clouds, ranging in size from giant molecular clouds (GMC) (with sizes of tens of parsecs, masses of up to millions solar masses, and mean hydrogen number densities of 100 - 1000 $\text{cm}^{-3}$) to small dense cores (with sizes of a few tenths of a parsec, subsolar masses, and mean hydrogen number densities of $\sim 10^4 - 10^6$ $\text{cm}^{-3}$) (Larson, 1981; Goldsmith, 1987). Measurements of CO emission lines reveal that the molecular clouds are generally extremely cold, T = 10 - 20 K (Goldsmith, 1987). The majority of the molecular clouds appear to

be bound by self-gravity (Larson, 1981; Myers, 1987; Maloney, 1990).

## 1.4   Magnetic fields

The interaction between magnetic fields and interstellar matter is happening through Lorenz force. While the magnetic fields can only act on charged particles, even the neutral gas phases contain a small fraction of ions that are able to transmit the effect of the magnetic field to neutral particles through neutral-ion collisions (Spitzer, 1958; Kulkarni & Heiles, 1987). In the densest parts of the molecular clouds, the ionization degree may be too low for this transmission (Shu et al., 1987).

Magnetic fields are important in supporting the ordinary matter against the Galactic gravitational potential at large scales. At small scales, they influence the turbulent motions of the gas, especially the formation of supernova shells, and help supporting the cold cores against collapse under self-gravity through magnetic pressure. In prestellar cores, the magnetic pressure is not enough to constrain the neutral gas via neutral-ion collisions, generally believed to be due to the low ionization degree, and thus the neutral gas flows inwards to eventually form a star (Nakano, 1979; Mestel, 1985).

While magnetic field direction can be derived from the linear polarization measurements of starlight or dust emission (see Section 2.1.5), the polarization vectors do not instantly tell us of the magnetic field strength. Chandrasekhar & Fermi (1953) proposed a method (Chandrasekhar-Fermi method or CF method) of deriving the absolute value of the magnetic field strength from the observed dispersion of the polarization angles and the gas velocity. This was done by assuming that the turbulent motions causing the magnetic field perturbations are Alfvénic and the rms velocity field is isotropic. Ostriker et al. (2001) suggested that the CF method might only be applicable when the dispersion is small ($<$ 25 deg) (see also Padoan et al., 2001). Heitsch et al. (2001) showed that the coarser resolution of the observations would reduce the observed dispersion and hence cause an overestimation of the magnetic field strength. Falceta-Goncalves et al. (2008) presented a new, more general formulation of the CF method, which performed well in their tests.

The Zeeman splitting measurements have been performed successfully since Vershuur (1969). Zeeman splitting of radio lines (e.g. H I 21-cm line) occurs due to the interaction of the external magnetic field with the magnetic moment of the valence electrons, causing a subdivision of certain energy levels. The amplitude of the splitting, $\Delta\nu$, is directly proportional to the magnetic field strength. Unfortunately, this splitting is usually small compared to the linewidth, making

it very hard to detect. Hence, the usual method is to observe the difference of the two circularly polarized components of the line radiation, which gives the strength of the line-of-sight magnetic field component. Due to the need for strong, narrow emission peaks, Galactic measurements are biased toward regions with high cold H I column density. In molecular clouds, lines of OH molecules in centimeter-range are often used.

Zeeman splitting measurements suggest that the strength of the ISM magnetic field is typically a few $\mu$G in regions with gas density $n = 1 - 100$ cm$^{-3}$ (see compilation by Troland & Heiles, 1986), increasing only slightly with $n$. In dense cores, $n = 10^2 - 10^4$ cm$^{-3}$, the effect is more pronounced, and the field strength may be as high as a few tens of $\mu$G (see also Myers et al., 1995; Crutcher, 1999; Troland & Crutcher, 2008). Falgarone et al. (2008) measured Zeeman effect on CN line in 14 regions of star formation, and reported a median value of $\sim 560\mu$G while the average density of the medium sampled was $n(\mathrm{H}_2) = 4.5 \times 10^5$ cm$^{-3}$.

Another method of deriving magnetic field strength is through Faraday rotation of linearly polarized radio signals. This method is biased toward ionized regions, where the free electrons cause the rotation of the $\mathbf{E}$ vector of the electromagnetic wave. Pulsars are often used as sources of the linearly polarized radiowaves. Based on Faraday rotation of polarized signal from pulsars, Rand & Kulkarni (1989) estimated that the local interstellar magnetic field has a uniform component of $\approx 1.6$ $\mu$G and a random component of $\sim 5$ $\mu$G.

The synchrotron emissivity depends on the magnetic field strength and the spectrum of cosmic ray electrons, neither of which has been reliably determined so far. However, the cosmic ray electron spectrum can be measured locally at Earth (Webber, 1983), and the local interstellar magnetic field strength is calculated to be $\approx 5.0$ $\mu G$ (see Ferriere, 2001).

## 1.5   Models

McKee & Ostriker (1977) presented a self-consistent, three-component model for the local ISM. Their model, however, had only individual supernovae, which therefore did not form the observed superbubbles. Later models that included the clustering of the supernovae (e.g. Heiles, 1990) found that the hot ionized gas had a filling factor of only $\sim 20\%$ in the solar neighborhood. Further MHD studies (e.g. Ferriere, 1998; Korpi et al., 1999) showed that not only is the filling factor sensitive to the supernova clustering, but it also varies strongly with the galactocentric radius (i.e., probability of supernovae explosions that create the hot ionized gas) and with the height from the galactic disk (the smaller gas pressure, the faster the expansion of supernova bubbles).

Table 1.1: Parameters for the different components of the ISM according to Scheffler & Elsässer (1988). $n$ is the number density, $T$ is the temperature and $f$ is the filling factor.

| Phase | $n$ [cm$^{-3}$] | $T$ [K] | $f$ |
|---|---|---|---|
| Cold molecular medium | $10^4$ | 20 | $5 \times 10^{-4}$ |
| Cold neutral medium | 20 | 80 | 0.020 |
| Warm neutral medium | 0.30 | 6000 | 0.200 |
| Warm ionized medium | 0.03 | 8000 | 0.100 |
| Hot ionized medium | $3.0 \times 10^{-3}$ | $6.5 \times 10^5$ | 0.70 |

Table 1.2: Average volume filling factors, $f$, in the disk ($-250$ pc $< z < 250$ pc) for the different ISM phases according to de Avillez & Breitschwerdt (2004). The results are based on three-dimensional supernova-driven ISM model, where the rate of the supernovae is the same as in our Galaxy. The disk-halo cycle is included, and the supernovae are clustered to the plane of the simulation, leading to much lower filling factor for the hot component in the disk.

| Phase | $T$ [K] | $f$ |
|---|---|---|
| Cold medium | $< 10^3$ | 0.19 |
| Cool medium | $10^3 - 10^4$ | 0.39 |
| Warm medium | $10^4 - 10^{5.5}$ | 0.25 |
| Hot medium | $> 10^{5.5}$ | 0.17 |

# Chapter 2

# Interstellar Dust

Interstellar dust makes up only a fraction of the interstellar matter, but it is the most visible sign of the ISM. Even with the naked eye, dark clouds can be seen against the bright starfield of the Milky Way, causing the obscuration of the background stars. Dust is formed in outer layers of evolved stars, in supernovae and possibly even in the ISM. Dust is everywhere where interstellar gas is, although dust grains can be broken up by energetic radiation and supernova shocks. Thus, the largest dust grains are to be found in dense clouds where they are shielded from radiation and can coagulate to form ever larger grains. The depletion of the heavier elements from the gas phase is most severe in cold, dense regions (Jenkins, 1987; Van Steenberg & Shull, 1988).

## 2.1 Extinction, scattering and emission

Trumpler (1930) measured the distances to numerous open clusters in the Galaxy using the apparent brightness of their most luminous stars and their absolute magnitude based on the spectral type, assuming a transparent interstellar medium. He then multiplied the angular size of the open cluster by the estimated distance and found that the clusters were systematically larger the farther away they were. Since this would put the Sun into a special position within the Galaxy, Trumpler argued that the light from the more distant clusters was dimmed by the intervening interstellar dust, even if there was not enough dust to block the light completely as had been the case with the dark clouds. Furthermore, he was able to show that with two stars of the same spectral class, the one farther away was redder than the closer one. This is because most of the grains are small, and thus scatter and absorb light more efficiently at shorter wavelengths, bluer wavelengths, than at longer, red wavelengths. Hence, the farther the light has to travel through the interstellar medium, the larger fraction of the short wavelength radiation is removed and the redder the star appears.
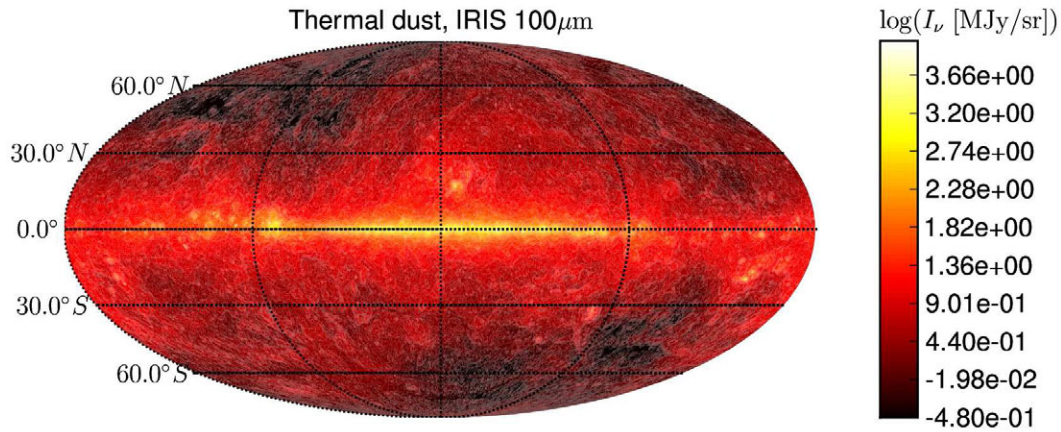
Figure 2.1: *IRAS* 100 $\mu$m dust map (IRIS reprocessed map, Miville-Deschenes & Lagache, 2005)

Interstellar dust is not evenly distributed over the sky. From measurements of the reddening and extinction toward different stars over the sky, it is possible to measure the column density of dust towards those stars. It was found that the column density of dust, while increasing with distance, is closely correlated with the hydrogen column density (Jenkins & Savage, 1974; Bohlin, 1975; Bohlin et al., 1978). Thus, the interstellar dust follows the inhomogeneous, patchy distribution of the interstellar gas.

### 2.1.1 Extinction curve

By doing measurements of the interstellar extinction toward an individual star at different wavelengths, it is possible to reconstruct the wavelength dependence of the extinction. This is called an extinction curve. Extinction curves are very important in deriving information about the dust size distribution and composition, as well as the spatial variance of those qualities.

In optical region, the slope of the extinction curve is usually expressed with a dimensionless quantity, $R_V \equiv A_V/(A_B - A_V)$. The average extinction law for diffuse regions of the Milky Way is characterized by $R_V \approx 3.1$ (Savage & Mathis, 1979; Cardelli et al., 1989), but $R_V$ varies from as low as 2.1 (Welty & Fowler, 1992) to as high as 5.6-5.8 (Cardelli et al., 1989; Fitzpatrick, 1999). Sightlines with dense clouds have a tendency for higher values of $R_V$, which can be due to grain growth by accretion and coagulation.

The most distinctive feature of the extinction curve is the broad bump at a UV wavelength $\approx$ 2175 Å, discovered by Stecher (1965). Immediately after that, Stecher & Donn (1965) suggested that absorption by small graphite grains would explain such a bump. The consensus is that this feature is probably due to some kind of graphite grain (e.g. Gilra, 1972; Mathis et al., 1977), although
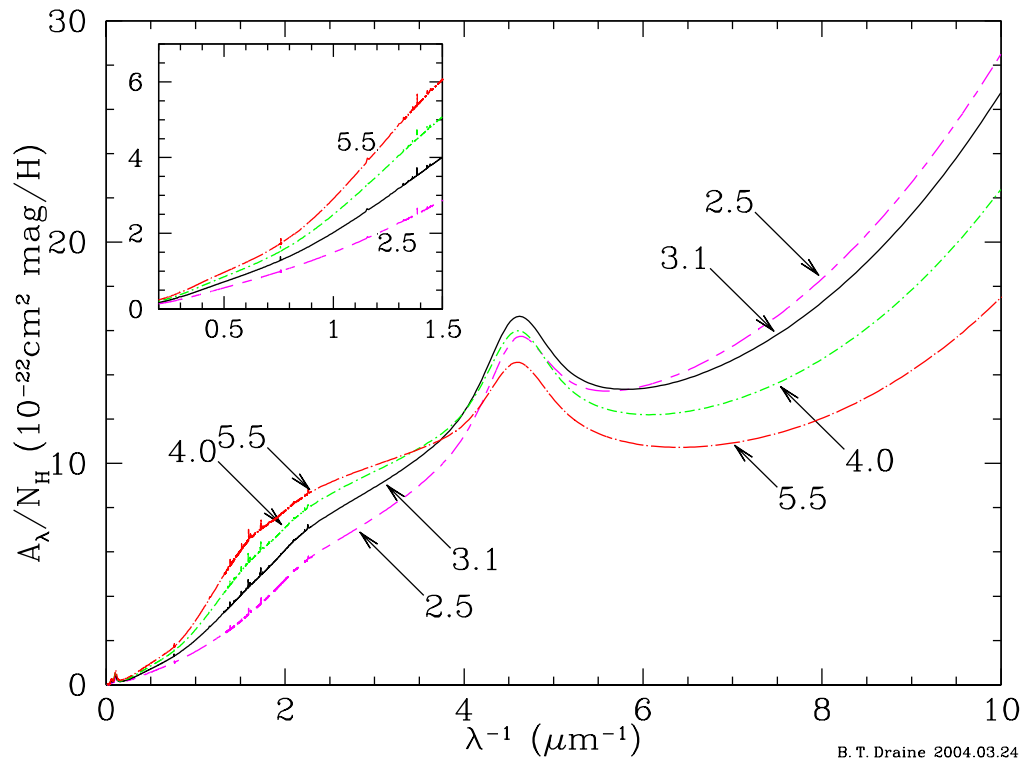
Figure 2.2: Extinction curve for different values of $R_V$, using Fitzpatrick (1999) extinction curve fit and Eq. 5 in Draine (2003a) to derive the $A_{IC}/N_H$ for each $R_V$. (Draine 2003a, erratum)

other suggestions are put forward as well (see Mathis, 1987, for a review). The grain models of Weingartner & Draine (2001) and Li & Draine (2001) have large polycyclic aromatic hydrocarbon (PAH) molecules that do produce the observed bump. The variation of the width of the bump between different sightlines could then be interpreted as differences in the PAH mix. Five emission features in mid-infrared (3.3, 6.2, 7.7, 8.6 and 11.3 $\mu$m) have been suggested to be due to PAHs as well (Duley & Williams, 1981; Leger & Puget, 1984), although the agreement with the laboratory spectra is not perfect.

In infrared extinction, there is a strong absorption feature at 9.7$\mu$m, which has been interpreted to arise from silicate minerals (Knacke & Thomson, 1973; Draine & Lee, 1984). Another feature at 18$\mu$m is likewise presumed to be of silicate origins (McCarthy et al., 1980; Smith et al., 2000). Due to the fact that the 9.7$\mu$m feature is broad and relatively featureless, laboratory experiments are in favor of interstellar amorphous silicate as the main contributor, with only a minor fraction of crystalline silicate (see Draine, 2003a). The 3.1 $\mu$m absorption feature, due to an O-H stretching mode in solid $H_2O$, appears in dense molecular clouds, implying that the dust is coated with ice within the cores (e.g. Whittet et al. 1988).

## 2.1.2  Scattering

Extinction consists of two processes: absorption, where the photon energy is turned into heat, and scattering, where the direction of the light propagation changes due to diffraction of light by small, solid bodies. For homogeneous spheres the problem of scattering was solved analytically by Gustav Mie in 1908. Programs such as DDSCAT (Draine & Flatau, 1994) can solve scattering numerically for irregular grains as well. Scattering is at its most efficient when the size of the grain is the same as the wavelength of the radiation. Scattering is often characterized with two parameters: albedo, which is the fraction of the extinction that is due to scattering, and scattering anisotropy factor, $g$, which is the mean value of the cosine of the angle of scattering.

Scattering by interstellar dust can be observed in three general situations: 1) "diffuse Galactic light" (DGL), which is scattering of the interstellar radiation field (ISRF) by the diffuse dust, strongly concentrated to the Galactic plane, 2) reflection nebulae, illuminated by a nearby, usually very bright star, 3) scattering of the ISRF by a dark cloud, usually at high enough Galactic latitude that its faint glow contrasts with a relatively dark sky background.

Optical DGL is quite faint and asymmetric in its angular distribution. Optical DGL was first detected by Elvey & Roach (1937). Henyey & Greenstein (1941) carried out verifying observations and found that the interstellar dust grains have relatively high albedos and are strongly forward scattering. They presented an analytic function to model anisotropic scattering with one parameter, $g$, and the so called Henyey-Greenstein phase function has been used widely ever since. Observations of DGL require careful correction for the contribution of faint stars, airglow and especially zodiacal light. The advantage of DGL is that the distribution of stars and the dust are well known, in contrast to reflection nebulae. For example, Witt (1968) used a model of the Galactic starlight to derive the grain properties from the observations of the DGL.

Reflection nebulae are much brighter than DGL, and the spectral properties of the radiation illuminating them are better known than the ISRF. However, the geometry of the reflection nebulae and their illuminating stars are not well known, causing problems with the interpretation of the scattering angle. The star might be in front of the cloud, in which case the scattering angle would be large, or the star could be embedded into the cloud or located behind the cloud, in which case the scattered light would be dominated by forward scattering by the grains on the line of sight. The reflection nebulae can be patchy, causing further problems.

The scattering by dark clouds was detected in optical wavelengths by Struve & Elvey (1936) and Struve (1937). The geometry is believed to be better known,

since the illumination source is the ISRF and not a single star. Mattila (1970a,b) determined the albedo and the scattering asymmetry parameter by comparing two dark clouds at different latitudes and assuming their dust to be similar. The UV scattering by a discrete diffuse cloud was first imaged by Haikala et al. (1995).

Of particular importance for this thesis is the scattered near-infrared (NIR) light in dark clouds illuminated by the ISRF. First detection was made by Lehtinen & Mattila (1996). They also found that the scattered light intensity in the $J$, $H$ and $K$ bands was linearly dependent on the column density up to optical depth $\sim 1$ in the wavelength band in question. The idea of using NIR surface brightness as an extinction estimator in dark clouds was presented by Lehtinen et al. in the ESO Press release 26a/2003. Nakajima et al. (2003) presented $JHK$ surface brightness maps of Lupus 3 dark cloud. Based on their analysis of $JHK$ surface brightness vs. $A_V$, they concluded that the surface brightness was due to scattered ISRF light by dust. Foster & Goodman (2006) observed in two dark clouds, L1448 and L1451, diffuse surface brightness which they attributed to NIR light scattered from dust particles. However, the observations were not made with extended emission in mind and, in the data reduction of the dithered observations, much of the diffuse emission was lost.

### 2.1.3 Absorption and emission

Interstellar dust grains are heated primarily by absorption of starlight. Collisional heating can dominate in dense regions in dark clouds where the starlight has been strongly attenuated, or in dense, hot, shocked gas. When a dust grain absorbs a starlight photon, the grain is rapidly heated up, and then it begins to cool again. Larger grains ($> 0.02$ $\mu$m) get heated less and they are hit by photons more often, keeping the temperature oscillating only slightly. Thus, it is possible to approximate them as having a steady temperature. However, small grains ($< 0.02$ $\mu$m) are heated very strongly by a single absorbed photon, and then can cool down again before another photon is absorbed. Most of the power emitted by small grains in the infrared is radiated when they are heated up, close to the peak of their temperature, complicating the calculations (see Draine & Li, 2001). In general ISM, the absorbed stellar photons heat the large grains to temperatures about 15 - 20 K, and the dust grains then re-emit the energy mostly in the far-infrared.

Infrared astronomy was started in the 1970s, but the major steps forward came during the 1980s with two satellite missions: the *Infrared Astronomy Satellite* (*IRAS*, 1983) and the *Cosmic Background Explorer* (*COBE*, 1989-90). Both satellites provided all-sky maps of the diffuse IR emission measured out-

side the atmosphere; *IRAS* with better spatial resolution (a few arc minutes at $12-100$ $\mu$m), while *COBE* had a broader spectral coverage and better absolute calibration. Boulanger & Perault (1988) showed that away from local heating sources, like bright stars, there is a good correlation between 100 $\mu$m IR emission outside molecular clouds and the H I column density, and between 100 $\mu$m IR emission from nearby molecular clouds and their $H_2$ column density. Schlegel et al. (1998) produced a composite all-sky map of 100 $\mu$m IR emission that combines the spatial resolution of *IRAS* with the *COBE* quality calibration.

The spectral coverage of *IRAS* was 12, 25, 60 and 100 $\mu$m. The *COBE* satellite had two instruments that are of interest to dust emission: Far Infrared Absolute Spectrophotometer (FIRAS), which covered the wavelengths from 0.1 to 10 mm, and Diffuse Infrared Background Experiment (DIRBE), which covered the wavelength range from 1.25 to 240 $\mu$m. While the resolution of *COBE* was poor in comparison to *IRAS* (0.7 degrees for DIRBE and 7 degrees for FIRAS), the large spectral coverage allowed the estimation of the large-scale dust emission spectrum beyond 100 $\mu$m. Boulanger et al. (1996) achieved a good fit by a Planck function with temperature $\approx 17.5$ K times an emissivity $\propto \lambda^{-2}$, although some features could not be fitted using a single temperature. Dwek et al. (1997) allowed for a realistic spread in grain temperature and were able to get a good fit for the range of $3.5-500$ $\mu$m, using a dust model with spherical graphite and silicate grains, and planar PAH molecules, illuminated by the local interstellar radiation field. In their model, the large graphite and silicate grains are responsible for emission beyond 140 $\mu$m, while the smaller particles, which are stochastically heated to momentary higher temperatures, provide the excess emission below 100 $\mu$m.

While the equilibrium temperature for the large grains seems to be fairly uniform $\approx 17.5$ K, large-scale far-IR maps reveal the presence of cold ($\approx 15$ K) dust statistically connected with molecular clouds (Lagache et al, 1998). In dense, nearby cloud cores the dust temperature has been observed to drop as low as 12 K (Ristorcelli et al., 1998; Bernard et al., 1999; Juvela et al., 2002; Lehtinen et al., 2003; Ridderstad et al., 2006). Even lower temperature values have been suggested (some cores in Lehtinen et al., 2003; Pagani et al., 2003). The dust and gas temperatures seem to be decoupled, at least outside dense cores. Lagache et al. (2000) concluded that the dust temperature and abundances in the warm ionized medium do not differ significantly from those in H I regions. However, Odegard et al. (2007) added a note of caution, as their analysis resulted in a value of 100 $\mu$m dust emissivity of warm ionized medium that was only 40% of the 100 $\mu$m dust emissivity of the neutral atomic medium.

*Planck* satellite, launched in May 2009, will provide all-sky maps for wavelength coverage comparable to FIRAS, but with much better resolution and
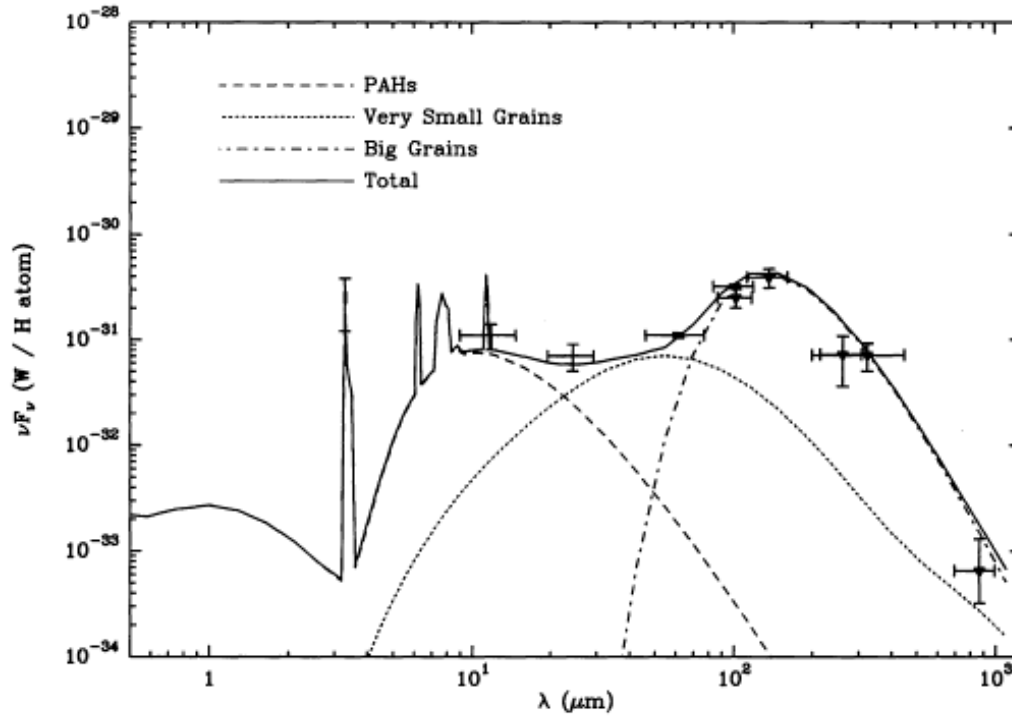
Figure 2.3: Dust emission spectrum from Desert et al. (1990), showing the components of their dust model. Observations (crosses) are for diffuse interstellar medium (see Table 1 in Desert et al., 1990), with the horizontal bar representing the filter width used in the observations.

sensitivity. Of particular interest for astronomers interested in interstellar dust are the three shortest wavelengths - 350, 550 and 850 $\mu$m - where the Galactic dust is expected to dominate the observed signal. Thanks to *Planck*'s resolution of 5 arc minutes at these wavelengths, it should be possible to distinguish small, dense cold cores from their warmer surroundings using the spectral information. *ARCHEOPS*, the balloon-borne precursor to *Planck*, found $\sim 300$ cold, submillimeter clumps from their survey, which covered $\sim 30\%$ of the sky (Desert et al., 2008).

### 2.1.4   Polarization

The linear polarization of starlight was discovered in mid-twentieth century (Hall, 1949; Hiltner, 1949). Soon there after, Davis & Greenstein (1951) proposed their paramagnetic relaxation model, where a rapidly spinning dust grain would align its spin axis parallel to the local magnetic field. If the grains are not spheres, the long axis of the projection of the spinning grain on the sky becomes perpendicular to the magnetic field. The light passing through is preferentially blocked along the long axis of the grain, and thus the observed light would show polarization coinciding with the direction of the magnetic field. While the paramagnetic model has come under severe criticism ever since and would not seem to be the dominant alignment mechanism, it is an observed fact that something does align the grains. Numerous theories have been offered over the years, and there is an excellent review by Lazarian (2007) on this topic.

The first large-scale polarization database was compiled by Mathewson & Ford (1970), consisting of almost 7000 stars distributed over both celestial hemispheres. Mathewson & Ford's catalog continued to be the best reference for over a quarter of a century, until finally superseded by the more complete catalog by Heiles (2000).

Serkowski (1973) presented an empirical fitting function ("Serkowski's law") to approximate the degree of polarization, $p$, as a function of wavelength, $\lambda$:

$$p(\lambda) = p_{\max} \exp[-K(\log(\lambda/\lambda_{\max}))^2], \tag{2.1}$$

where $\lambda_{\max} \approx 5500$ Å and $K \approx 1$ for most sightlines through diffuse clouds. The wavelength $\lambda_{\max}$ has been shown to correlate with $R_V$ (Clayton & Mathis, 1988), while $K$ depends on the value of $\lambda_{\max}$ (Wilking et al., 1982). Serkowski's law fits the observational data well for $0.8\mu\text{m}^{-1} \leq \lambda^{-1} \leq 3\mu\text{m}^{-1}$. UV observations (Anderson et al., 1996; Clayton et al., 1996; Wolff et al., 1997) reveal that the degree of polarization continues to drop with shorter wavelengths, implying that the small grains responsible for the extinction in UV are either nearly spherical or minimally aligned (Kim & Martin, 1995).

Near-infrared stellar polarimetry is able to probe lines of sight intercepting dense cores. In such regions the polarization per unit extinction declines systematically with optical depth (Goodman et al., 1992, 1995; Gerakines et al., 1995). The implication is that grains within the clouds are less well aligned than in the diffuse ISM. Whittet et al. (2008) studied the near-IR polarization of stars seen through dense clouds, and concluded that the grain alignment by radiative torques offered the best explanation for the data.

The thermal emission of aligned dust grains at far-infrared and longer wavelengths is polarized, since the grains are more efficient radiators along their long axis. Hence, while the starlight is polarized along the magnetic field lines, the thermal dust emission is polarized perpendicular to the magnetic field. In the literature, however, it is customary to plot the direction of the magnetic field rather than the direction of the polarized emission. Numerous observations of dense clouds have been done at various wavelengths, finding linear polarization degrees as large as 10% (e.g. Lai et al., 2001). Interestingly, Hildebrand et al. (1999) found that the wavelength dependence of the measured polarization implies that the grain alignment efficiency is higher in warmer regions. Similarly, Ward-Thompson et al. (2000) and Henning et al. (2001) found that the observed polarization degree drops towards the densest part of a cloud (see Fig. 2.4). Chapter 4 will pick up this topic.

## 2.2   Dust models

The composition of dust has already been mentioned in relation to the extinction curve. Mathis et al. (1977) suggested a simple power-law distribution of graphite and silicate, to reproduce the observed extinction curve from 0.11 to 1.1 $\mu$m for lines of sight passing through diffuse clouds. In their model (called MRN), the graphite and silicate grains were from 0.005 to 0.25 $\mu$m in size and the size distribution was given by

$$dn = n(a)da = Cn_{\mathrm{H}}a^{-3.5}da, \;\; a_{\min} < a < a_{\max}, \tag{2.2}$$

where $n(a)$ is the number density of grains with size in the interval $[a, a + da]$, and $n_{\mathrm{H}}$ is the number density of H nuclei (in both atoms and molecules). Draine & Lee (1984) provided the following normalizations of the size distribution: $C = 10^{-25.13}(10^{-25.11})$ cm$^{2.5}$ for graphite (silicate).

A more sophisticated model was presented in two papers by Weingartner & Draine (2001) and Li & Draine (2001). In this model, there were still two basic components: graphite and silicate. However, the graphite component had two additional grain populations: one peaking at $\sim 6$ Å to account for PAH emission
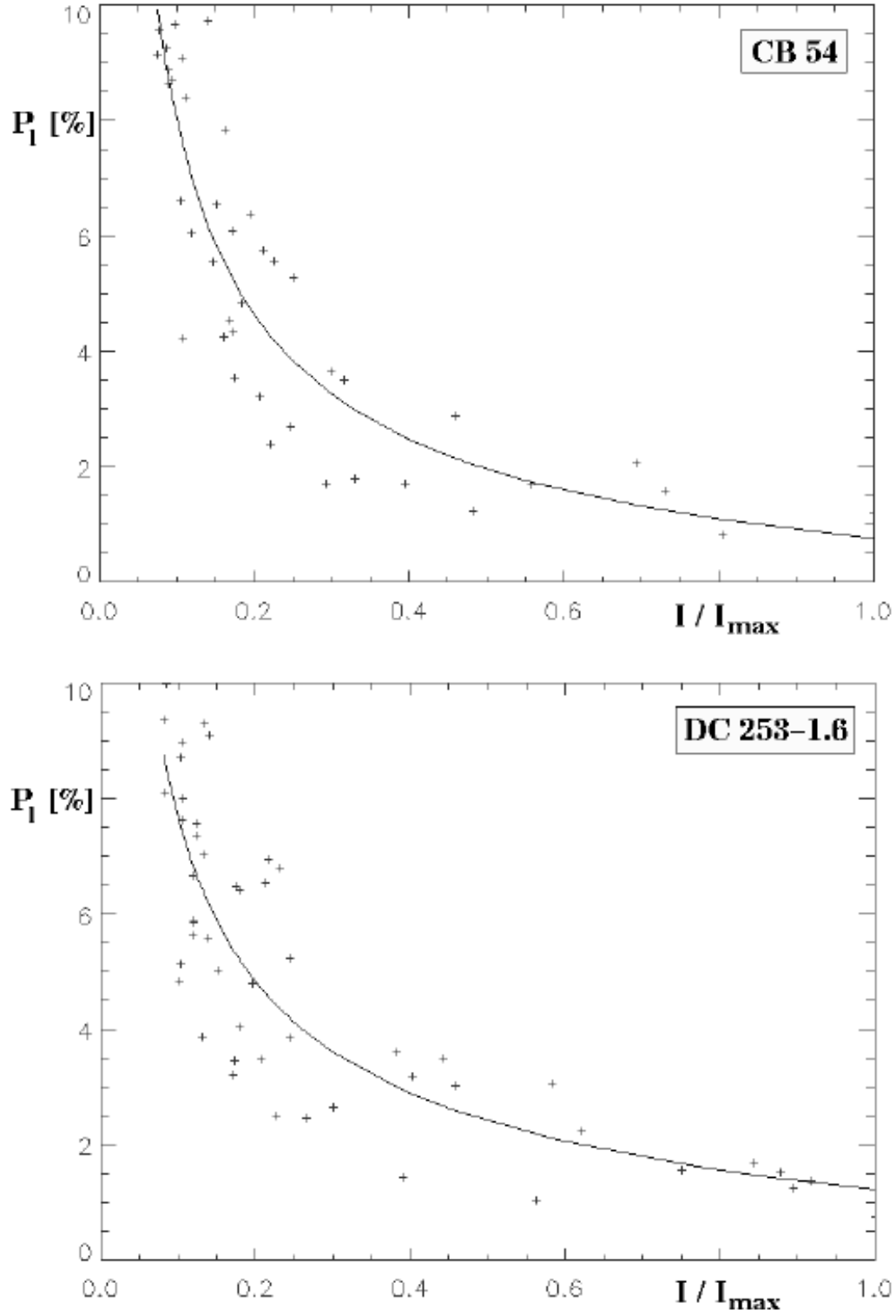
Figure 2.4:   Distribution of polarization degree, $P_1$, vs. total intensity, $I$, at wavelength 850 $\mu$m in two cores by Henning et al. (2001).

features and the other peaking at $\sim 50$ Å to account for the 60 $\mu$m flux. The very small graphite grains were assumed to have PAH-like properties, while those $> 50$ Å were assumed to have graphitic properties. The model was able to reproduce the observed extinction curves for different $R_V$:s by varying the parameters of the size distributions (Weingartner & Draine, 2001). The model also has a set of dust properties for the grains, and using the observed interstellar extinction, the model was able to reproduce the observed near-IR to submillimeter emission of the diffuse interstellar medium (Li & Draine, 2001). In addition, Li & Draine (2001) found that the total infrared emission of their model was in excellent agreement with *COBE*/DIRBE observations at high latitude, and the albedo was consistent with the observations of the diffuse interstellar medium. Draine (2003b) compared the phase function calculated from the dust model to Henyey-Greenstein phase function (Henyey & Greenstein, 1941). He found that while there was a good agreement in the wavelength range 0.4 $\mu$m $< \lambda < 1$ $\mu$m, the functions differed at shorter and longer wavelengths, which prompted him to propose a new analytical function.

Another grain model was offered by Ossenkopf & Henning (1994), based on MRN size distribution. They studied how the grain coagulation and the formation of ice mantles onto the grains, both of which happen in dense cloud cores, influence the opacity of the grains. Because the depletion of molecules onto the grains to form ice mantles happens quickly compared to the coagulation, they had three ice mantle models: 1) thick ice mantles, corresponding to a case where all volatile molecules in the gas phase have depleted into ice mantles, 2) thin ice mantles, corresponding to a more realistic case and based on observational evidence, and 3) grains without ice mantles, as a limiting case or corresponding to a case where grains have been warmed up but not destroyed themselves. The grains are then allowed to coagulate in different density environments for $10^5$ years, which may be longer than the free-fall time of a collapsing cloud core. As the result of the grain growth by grain coagulation, Ossenkopf & Henning (1994) found that the opacity in the sub-millimeter could grow by a factor of 4-5. The Ossenkopf & Henning dust model is often used when modelling dense dust cores where coagulation has taken place.

# Chapter 3

# Column density estimates of interstellar dust clouds

Interstellar clouds are complex structures, created by the interaction of supersonic turbulent flows with magnetic and gravitational forces. The observations of cloud structure provide evidence on the relative importance of turbulence, magnetic fields, and self-gravity, and thus give constraints to the models of star formation.

There are many methods to derive the column density of a cloud, for example: 1) the integrated intensity of molecular or atomic line emission (e.g. Padoan et al., 1999), particularly CO and H I, 2) star counts of optical (e.g. Wolf, 1923; Barnard, 1927) or near-infrared (NIR) wavelengths, 3) the thermal emission of dust grains at far-infrared and sub-millimeter wavelengths (e.g. Schlegel et al., 1998), 4) the optical or near-infrared reddening of the background starlight (e.g. Lada et al., 1994; Lombardi & Alves, 2001), and 5) the optical or near-infrared scattered light (Papers I-IV). All these methods have their uses, but they also have their limitations. The first two are briefly discussed below while the latter three are covered in more detail in the following sections.

A molecular line is sensitive to a certain density interval: dense enough to be self-shielded from destruction by radiation field, but not so dense as to saturate the line due to the large optical depth. The molecular abundances depend on a complicated network of time-dependent chemical reactions that are affected by turbulent transport and depletion on dust grains. As the result, different molecular tracers may peak at different parts of the cloud, influencing the column density map. Single dish resolutions are typically limited to some tens of arc seconds, with arc second resolutions achieved only by interferometric observations.

Optical star counts are limited by the fact that the number of observed stars in a resolution element drops rapidly after $A_V \sim 1^m$, reaching the limit of usefulness around $A_V \sim 5^m$. As a statistical method, a large number of stars is needed for

each resolution element. This gives a poor resolution even when using near-infrared star counts, which can extend to $A_V \sim 20^m$.

## 3.1 The method using thermal dust emission

Thermal dust emission seems like a more straightforward approach to derive the column density map, but it requires that the dust temperatures can be estimated and that the dust to gas ratio stays constant. Both of these may have significant spatial variations (e.g. Cambresy et al., 2001; Dupac et al., 2003; Ridderstad et al., 2006) due to grain growth by coagulation and ice mantle deposition (Ossenkopf & Henning, 1994) or physical changes in the grain material (e.g. Mennella et al., 1998; Boudet et al., 2005). The low intensity of clouds without internal heat sources limits the observations to high column density regions, typically $A_V \sim 10^m$ or above. Spatial resolution is of the order of 10".

Dust temperature can be derived if observations have been made with two far-infrared (FIR) wavelengths. At wavelengths in excess of 100 $\mu$m, the large grains are thought to be the dominant source of emission (see Fig. 2.3), and it is feasible to attribute a single equilibrium temperature to the dust. In general, the opacity, $\kappa_\nu$, follows a power law in FIR, $\kappa_\nu \propto \nu^\alpha$, where $\alpha$ depends on the dust properties. Observations show that $\alpha$ varies with temperature and wavelength. While observing cold clouds ($T < 20$ K) in sub-millimeter, Dupac et al. (2003) found $\alpha = 2.0 \pm 0.4$. Since the ISM is optically thin in FIR, the intensity of the thermal dust emission $I_\nu$ is given by

$$I_\nu = N_d \kappa_\nu B_\nu(T), \tag{3.1}$$

where $N_d$ is the column density of dust in g cm$^{-2}$, and $B_\nu(T)$ is the Planck function (black-body intensity) at temperature $T$ and frequency $\nu$.

If we take $\alpha = 2$, we can write

$$\frac{I_{\nu_1}}{I_{\nu_2}} = \frac{N_d \kappa_{\nu_1} B_{\nu_1}(T)}{N_d \kappa_{\nu_2} B_{\nu_2}(T)} = \frac{B_{\nu_1}(T)\nu_1^2}{B_{\nu_2}(T)\nu_2^2}, \tag{3.2}$$

where $I_{\nu_1}$ and $I_{\nu_2}$ are the observed intensities at frequencies $\nu_1$ and $\nu_2$. This is the idealized case, as the filters have a passband of finite size. However, the passband is usually well known, and a correction term can be included. Once the temperature is solved from Eq. 3.2, and $\kappa_\nu$ is either fixed from other column density measurements, or by assuming a certain dust model, we can calculate $N_d$ from Eq. 3.1. By assuming a specific dust model, $N_d$ can be transformed to visual extinction, $A_V$, and using an empirical law by Bohlin et al. (1978), the column density of neutral hydrogen can be derived from $A_V$. Alternatively, a dust-to-gas ratio can be assumed in which case the column density of neutral hydrogen is derived by simple multiplication from $N_d$.

## 3.2  NICER method

Lada et al. (1994) pioneered the Near-Infrared Color Excess (NICE) method, which used the NIR color excesses for individual stars through the cloud. The intrinsic NIR colors of the stars have relatively low scatter, and the mean intrinsic NIR color can be measured from a large sample of stars in a nearby field where the extinction is negligible. The two main limitations of NICE method are the scatter of the color due to photometric errors and intrinsic scatter, and the inclusion of foreground stars which are bluer than the background stars, biasing the result.

Lombardi & Alves (2001) presented the Near-Infrared Color Excess Revised (NICER) method, which expanded the NICE method to an optimized multi-band method using three wavelengths (in their case $J$, $H$ and $K$) or, in principle, more than three wavelengths. In the following, the formalism of Lombardi & Alves (2001) is used.

With three wavelengths, two independent color indices can be formed: $c_1 = J - H$ and $c_2 = H - K$. For each color, the relationship between the observed color, $c_i^{\mathrm{obs}}$, and the intrinsic, true color, $c_i^{\mathrm{tr}}$, is

$$c_i^{\mathrm{obs}} = c_i^{\mathrm{tr}} + k_1 A_{\mathrm{V}} + \epsilon_i, \tag{3.3}$$

where $k_i = E_i/A_V$ is the ratio between the color excess on the band $i$ and the extinction in the $V$ band (for example, Lombardi & Alves (2001) quoted values $k_1 = 1/9.35$ and $k_2 = 1/15.87$), and $\epsilon_i$ is the error of the color index resulting from photometric errors.

The extinction estimate, $\hat{A}_{\mathrm{V}}$, for a single star is given by

$$\hat{A}_{\mathrm{V}} = a + b_1 c_1^{\mathrm{obs}} + b_2 c_2^{\mathrm{obs}}. \tag{3.4}$$

The coefficients $a$, $b_1$, and $b_2$ are derived from two conditions:
1) the estimator is unbiased, i.e. its expected value is the true extinction $A_{\mathrm{V}}$, and
2) the estimator has minimum variance.
The variance of $\hat{A}_{\mathrm{V}}$ is

$$\mathrm{Var}(\hat{A}_{\mathrm{V}}) = \sum_{i,j} b_i b_j \mathrm{Cov}_{ij}(c^{\mathrm{tr}}) + \sum_{i,j} b_i b_j \mathrm{Cov}_{ij}(\epsilon), \tag{3.5}$$

where the first covariance matrix, $\mathrm{Cov}_{ij}(c^{\mathrm{tr}})$, is the scatter of intrinsic star colors that can be determined from the control field, and $\mathrm{Cov}_{ij}(\epsilon)$ is related to photometric errors. The optimal estimator is

$$\hat{A}_{\mathrm{V}} = b_1[c_1^{\mathrm{obs}} - \langle c_1^{\mathrm{tr}} \rangle] + b_2[c_2^{\mathrm{obs}} - \langle c_2^{\mathrm{tr}} \rangle], \tag{3.6}$$

where $b_1$ and $b_2$ are given by variance minimization (for details, see Lombardi & Alves, 2001), and $\langle c_i^{\mathrm{tr}} \rangle$ are the mean colors of the control field.

The final extinction map is obtained by spatially smoothing the individual extinction estimates. One method is to use a weighted mean of the estimators with a Gaussian beam. The extinction towards direction $\Theta$ on the sky is given by

$$\hat{A}_{\mathrm{V}}(\Theta) = \frac{\sum\limits_{n=1}^{N} W^{(n)} \hat{A}_{\mathrm{V}}^{(n)}}{\sum\limits_{n=1}^{N} W^{(n)}}, \tag{3.7}$$

$$W^{(n)} = \frac{W(\Theta - \Theta^{(n)})}{\mathrm{Var}(\hat{A}_{\mathrm{V}}^{(n)})}, \tag{3.8}$$

where $\Theta^{(n)}$, $W^{(n)}$, and $\hat{A}_{\mathrm{V}}^{(n)}$ are the direction, weight and extinction estimate of the $n$th star, respectively, $N$ is the number of all observed stars in the field, and $W(\Theta - \Theta^{(n)})$ is the Gaussian weight function. The width of $W$ sets the effective resolution of the derived extinction map and the signal-to-noise ratio: a large width gives a smooth map with a poor resolution, while a small width gives a noisy map with a high resolution. The choice of an appropriate width depends on the depth of the observations and the stellar density of the background. With deep, dedicated observations it is possible to reach even 10". With *2MASS* data, observations towards the Galactic bulge can have a resolution of an arc minute (e.g. Lombardi et al., 2006), while for high latitude clouds the resolution is of the order of a few arc minutes (e.g. Cambresy et al., 2002; Kainulainen et al., 2006; Lombardi et al., 2008).

The problem of the foreground stars can be alleviated by a method called sigma-clipping. The local estimate of the error is

$$\sigma_{\hat{A}_{\mathrm{V}}}^2(\Theta) = \frac{\sum\limits_{n=1}^{N} (W^{(n)})^2 \mathrm{Var}(\hat{A}_{\mathrm{V}}^{(n)})}{\sum\limits_{n=1}^{N} (W^{(n)})^2}, \tag{3.9}$$

Sigma-clipping is done by calculating $\hat{A}_{\mathrm{V}}(\Theta^{(n)})$ and $\sigma_{\hat{A}_{\mathrm{V}}}$ for each star, and if the star's $\hat{A}_{\mathrm{V}}^{(n)}$ differs from the average by more than a factor of a few $\sigma_{\hat{A}_{\mathrm{V}}}$, it is removed and a new extinction value is calculated for the remaining stars until the two extinction estimates converge.

The NICER method is quite a robust extinction estimator, but it is not without its own limitations. The influence of foreground stars is expected to be insignificant in close-by ($d \leq 200$ pc) clouds (Lombardi et al., 2008), and easily detected and removed in high density regions (Lombardi & Alves, 2001). A harder problem is the substructure of the cloud below the resolution level.

If there are steep extinction gradients within the Gaussian beam, the stars are preferentially seen through the lower extinction part, and this biases the resulting extinction estimate downwards. Lombardi (2005) described this bias in detail, estimating it to be $\sim 1^{\mathrm{m}}$ at $A_{\mathrm{V}} = 15^{\mathrm{m}}$, and a subsequent paper (Lombardi 2009) proposed an improved method (NICEST) to correct for the substructure.

## 3.3 Method using the near-infrared scattered light

A new method of mapping interstellar clouds was proposed in Paper I, based on the NIR scattering of the ISRF. While optical and UV scattering could be used to probe regions of low $A_{\mathrm{V}}$, NIR scattered light could provide unparalleled spatial resolution down to arc second scales, and trace the column densities within a range of $A_{\mathrm{V}} = 1 - 20$ mag. In this method, it is assumed that the observed cloud is illuminated by an isotropic external radiation field, and the observed intensity can be attributed to scattering. It is furthermore assumed that the dust properties and, naturally, also the dust to gas ratio remains constant.

If the sightline through the cloud is optically thin at the wavelength in question, the scattered intensity directly depends on the column density. The scattered light starts to saturate approximately at 5, 10 and 20 mag of $A_{\mathrm{V}}$ for $J$, $H$ and $K$ band, respectively. The radiative transfer process can be divided to two phases. In the first phase, the external radiation penetrates the cloud and upon reaching the selected sightline, it is scattered toward the observer. In the second phase, the radiation travels along the selected sightline towards the observer and the intensity is reduced by both absorption and scattering.

The method concentrates on the second phase of the radiative transfer process. While the radiation is attenuated already in the first phase, it is likely that in a patchy cloud, the sightline can be illuminated through some lower density regions. In addition, most of the scattering is to forward direction, which also helps the radiation to reach the depths of the cloud.

If the relation between the observed intensity, $I$, and the column density, $N$, depends mainly on the second phase, radiative transfer equation along one line of sight in a homogeneous medium gives

$$I = a[1 - \exp(-bN)], \tag{3.10}$$

where the coefficients $a$ and $b$ are positive constants for each band and are related to the strength of the illuminating radiation field and to the dust properties. At small column densities, the formula reduces to

$$I = abN, \tag{3.11}$$
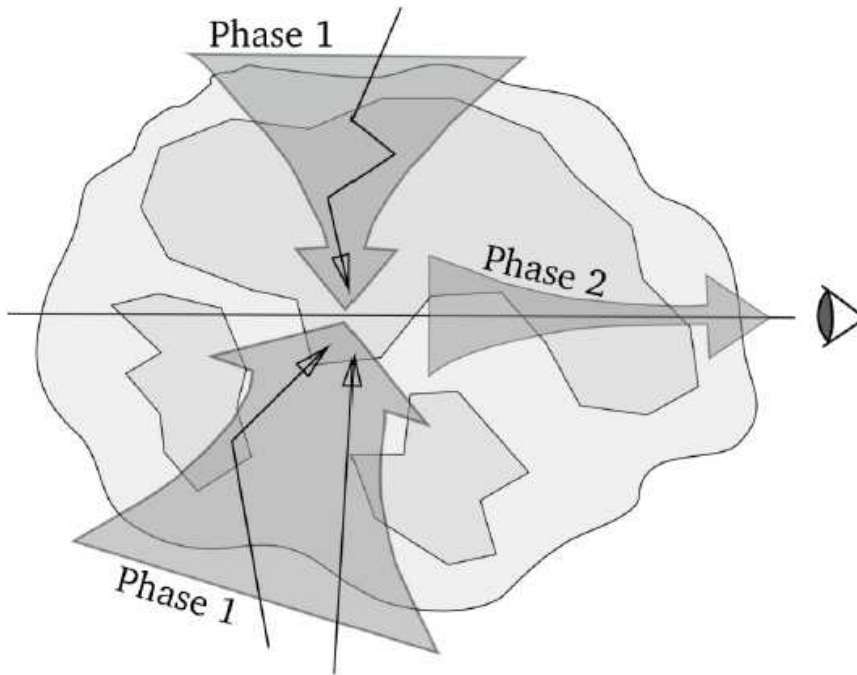
Figure 3.1:   Schematic representation of the two phases of scattering referred to in the text. (Paper II)
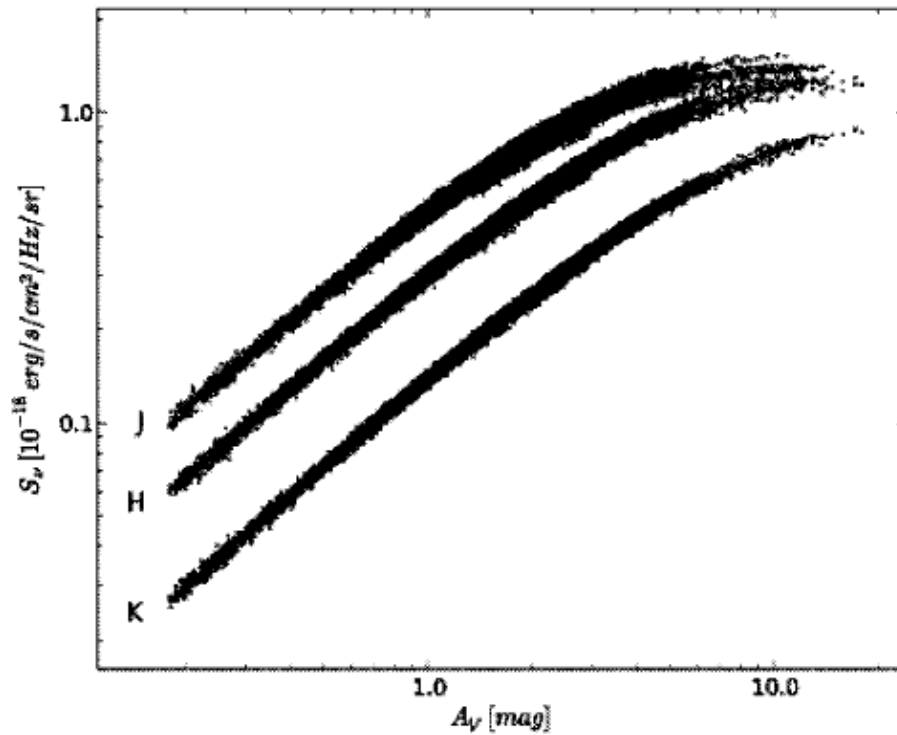


Figure 3.2:   The intensity of the scattered light vs. the true column density obtained from Monte Carlo radiative transfer calculations. The scatter is due to the variations of the impinging radiation field caused by the shadowing of dense regions within the 3D cloud model. (Paper I)

which gives a linear dependence of the intensity on the column density. Even though the intensity saturates at larger column densities, the different curvature of the intensities in each band still allow us to reconstruct the column density. Equation 3.10 can be written for each band separately, defining a parametric curve in $(I_J, I_H, I_K)$-space. Each sightline observed in $JHK$ bands can be assigned to a point on this curve by minimizing the least square distance from the curve. If constants $a$ and $b$ are known, the column density can be solved for each band separately:

$$N = -\frac{1}{b}\ln(1 - I/a). \tag{3.12}$$

Because $J$ band usually has a better signal-to-noise ratio at low $A_V$ but saturates first at high $A_V$, the relative weight given to the different bands should take this into account (if all the bands have the same signal to noise ratio, it was found in Paper II that the optimal result was obtained by choosing the weights 1:3:12 for $J : H : K$).

In the absence of independent column density estimates, the surface brightness observations can still be used to derive information on the dust properties. For example, the $H$ band intensity can be expressed in terms of the $K$ band one as

$$I_H = a_H \left[ 1 - \left( 1 - \frac{I_K}{a_K} \right)^{b_H/b_K} \right]. \tag{3.13}$$

The constants $a_J$, $a_H$, and $a_K$ and the ratios $b_J/b_K$ and $b_H/b_K$ can be derived by fitting this curve to the observations. The $b$ constants are expected to depend mainly on the properties of the dust grains, which vary only relatively little in NIR. Thus, it might be possible to use values derived from observations of one object to the analysis of other similar objects. The $a$ constants depend mainly on the radiation field illuminating the cloud. While the uncertainly of the intensity is often large, $\sim 50\%$, this affects mainly the absolute scaling of the column density map. The spectral shape of the incoming radiation might be different as well, if there are additional radiation sources nearby. However, if the $b$ constants are known, it is relatively trivial to estimate the spectrum from the linear part of the curve in low extinction sightlines. The expected values of $a$ and $b$ constants can also be derived from radiative transfer modelling, and the observations can be used to correct the values. Such a correction would be interesting on its own, since it implies that either the radiation field or the NIR dust properties differed from the assumed values.

As a by-product of the surface brightness observations, the observed fields contain data on a large amount of background stars. It is possible to use the NICER method on these stars and, even if the resolution would probably be

lower, it is enough to check the parameters and even to determine the values of individual $b$ constants. Furthermore, the error sources of the two methods should be different, and thus a comparison between the two methods will provide a test for the derived column density map. Nakajima et al. (2008) used the color excesses of individual stars to form an empirical function between the surface brightness and color excess, and derived a column density map from the surface brightness that way.

In Paper II, the accuracy of the method is carefully tested. Numerical simulations showed that the pixel-to-pixel errors were below 10% when the maximum extinction was below $A_V \sim 15^m$, although this requires similarly accurate parameters for Eq. 3.10. This can usually be accomplished with comparison with the stellar color excess data. Spatial variations of the dust properties were found to cause errors, but still below the 10% level. Large variations in the dust properties and in the external radiation field can cause large systematic errors, if left uncorrected, but the morphology of the map is usually reliable. Iterative radiative transfer modelling can be used to examine the effect that these variations would have on the observed cloud, and thus to refine the column density estimate.

NIR scattering could make it possible to reach sub-arc second scales with dedicated observations using large telescopes. At the distance of the closest interstellar clouds, $\sim 150$ pc, such spatial resolution would be on the scale of the size of circumstellar disks, i.e. $\sim 100$ AU. This makes NIR scattering a very useful tool in mapping interstellar clouds and examining the formation of cores, providing new perspectives into the small-scale processes of star formation.

# Chapter 4

# Polarized thermal dust emission and grain alignment by radiative torques

The polarization of thermal dust emission gives information on the morphology and the strength of the magnetic field within the cloud, and possibly also of the grain size distribution inside the cloud. The mechanisms of the far-infrared thermal emission are quite well understood (see Sections 2.1.3 and 3.1), and the polarization is due to the alignment of the grains with the magnetic field (see Section 2.1.4). However, what mechanisms align the grains? That question has been in the forefront of the debate for the last half century.

The theories of grain alignment mechanisms usually start by looking at a single dust grain. However, we do not observe a single dust grain, but the accumulated thermal emission of the grains along the line of sight. Thus, if a theory indicates that a grain could be aligned by a certain mechanism, we have to calculate the predicted polarized thermal emission, and compare our result with the observed polarization.

Amongst the many theories of grain alignment (see review by Lazarian, 2007), the strongest candidate is the radiative torque alignment. Dolginov (1972) noted that the interstellar grains might have different absorption and scattering cross sections for left- and right-handed circularly polarized light, thus resulting in a change in the grain angular momentum if illuminated by unpolarized, but anisotropic, radiation. Dolginov & Mytrophanov (1976) proposed further that this process could lead to rapid rotation and possible alignment of the grain. However, since they were unable to calculate the torques on grains with realistic compositions and sizes, the idea did not gain wide acceptance.

After the radiative torque alignment mechanism had been neglected for two decades, Draine & Weingartner (1996) (hereafter DW96) used numerical calcu-

lations to show that the efficiency of the radiative torques was sufficient to spin up the grains, although they made a mistake in assuming that the alignment itself might be via paramagnetic relaxation. In their subsequent paper, Draine & Weingartner (1997) demonstrated the ability of the radiative torques to align grains without paramagnetic relaxation.

## 4.1 Radiative torques in the Draine & Weingartner (1996) formalism

A grain, rotating with angular velocity $\omega$ around axis $\hat{\mathbf{a}}_1$ in neutral gas of hydrogen with density $n_H = n(H) + 2n(H_2)$ and temperature $T$, experiences a gas drag torque,

$$\mathbf{\Gamma}_{\text{drag,gas}} = -\frac{2}{3}\delta\left(1.2n_H\right)\left(8\pi m_H kT\right)^{1/2} a_{\text{eff}}^4 \omega\hat{\mathbf{a}}_1,\tag{4.1}$$

where $a_{\text{eff}}$ is the radius of a sphere of equal volume to the grain, $m_H$ is the mass of an H atom. $\delta$ depends on the manner of collisions by the impinging atoms, and on the shape of the grain (see DW96 for details). In general, $\delta \approx \alpha_1$, where $\alpha_1 = \frac{15I_1}{8\rho a_{\text{eff}}^5}$, $I_1$ the moment of inertia associated with axis $\hat{\mathbf{a}}_1$ and $\rho$ the solid density of the grain. The factor of 1.2 takes into account helium with $n_{He} = 0.1n_H$. The rotational damping time due to gas drag is:

$$\begin{aligned}\tau_{\text{drag,gas}} &= \frac{\pi\alpha_1\rho a_{\text{eff}}}{3\delta n_H\left(2\pi m_H kT\right)^{1/2}}\\ &= \left(8.74\times10^4\text{ yr}\right)\times\frac{\alpha_1}{\delta}\rho_3 a_{-5}T_2^{1/2}\left(\frac{3000\text{ cm}^{-3}\text{ K}}{n_H T}\right),\end{aligned}\tag{4.2}$$

where $\rho_3 = \rho/3$ g cm$^{-3}$, $a_{-5} = a_{\text{eff}}/10^{-5}$ cm, and $T_2 = T/10^2$ K. The rotational damping time due to thermal emission of photons by a grain heated by starlight to a temperature $T_d$, and the absorption efficiency factor $Q_{\text{abs}} \propto \lambda^{-\beta}$ with $\beta = 2$, is:

$$\begin{aligned}\tau_{\text{drag,em}} &= \frac{8\alpha_1\left(\beta+3\right)}{5}\frac{\zeta\left(\beta+4\right)}{\zeta\left(\beta+3\right)}\frac{\rho a_{\text{eff}}^3\left(kT_d\right)^2}{\hbar^2 c u_{\text{rad}}\langle Q_{\text{abs}}\rangle}\\ &= \left(1.60\times10^5\text{ yr}\right)\frac{\alpha_1\rho_3 a_{-5}^3}{\langle Q_{\text{abs}}\rangle}\left(\frac{T_d}{18\text{ K}}\right)^2\left(\frac{u_{\text{ISRF}}}{u_{\text{rad}}}\right),\end{aligned}\tag{4.3}$$

where $\zeta(x)$ is the Riemann $\zeta$-function, $u_{\text{ISRF}}$ and $u_{\text{rad}}$ are the energy density of interstellar radiation field outside the cloud (Mathis et al., 1983) and the radiation field illuminating the grain, respectively, and

$$\langle Q_{\text{abs}}\rangle = \frac{1}{u_{\text{rad}}}\int u_\lambda Q_{abs}(\lambda)\,d\lambda,\tag{4.4}$$

where $u_\lambda$ **is the energy density of the radiion field illuminating the grain at wavelength** $\lambda$. The damping due to absorption of starlight photons is negligible (Purcell 1979). The rotational damping time $\tau_{\text{drag}}$ can be calculated from:

$$\tau_{\text{drag}}^{-1} = \tau_{\text{drag,gas}}^{-1} + \tau_{\text{drag,em}}^{-1}. \tag{4.5}$$

If the grain is illuminated by a unidirectional radiation field with energy density $\gamma u_{\text{rad}}$, and by isotropic radiation field, $(1 - \gamma)u_{\text{rad}}$, the radiative torque along the rotation axis $\hat{\mathbf{a}}_1$ is given by:

$$\mathbf{\Gamma}_{\text{rad}} = \pi a_{\text{eff}}^2 u_{\text{rad}} \frac{\bar{\lambda}}{2\pi} \left[(1 - \gamma)\langle Q_\Gamma^{\text{iso}}\rangle + \gamma\langle \mathbf{Q}_\Gamma(\Theta, \Phi)\rangle \cdot \hat{\mathbf{a}}_1\right] \hat{\mathbf{a}}_1, \tag{4.6}$$

where

$$\bar{\lambda} \equiv \frac{\int \lambda u_\lambda d\lambda}{\int u_\lambda d\lambda}, \tag{4.7}$$

$$\langle \mathbf{Q}_\Gamma(\Theta, \Phi)\rangle \equiv \frac{\int \mathbf{Q}_\Gamma(\Theta, \Phi)\lambda u_\lambda d\lambda}{\int \lambda u_\lambda d\lambda}, \tag{4.8}$$

where $Q_\Gamma^{\text{iso}}$ and $\mathbf{Q}_\Gamma(\Theta, \Phi)$ are the radiative torque efficiencies (dimensionless) due to the isotropic and unidirectional radiation fields, respectively, $\Theta$ is the angle between the rotation axis of the grain and the propagation direction of the unidirectional radiation, and $\Phi$ is the azimuth angle of the rotation axis with respect to the propagation direction of the unidirectional radiation. Thus, $\Theta$ and $\Phi$ identify the orientation of the rotation axis of the grain in a scattering coordinate system. $Q_\Gamma^{\text{iso}}$ and $\mathbf{Q}_\Gamma(\Theta, \Phi)$ depend on the shape, properties and the size of the grain as well as the spectrum of the impinging radiation (see Table 4 in Draine & Weingartner, 1996). For example, for a silicate grain of $a = 0.05$ nm illuminated by the interstellar radiation field, $Q_\Gamma^{\text{iso}} = 2.75 \times 10^{-5}$ and $\hat{\mathbf{a}}_1 \cdot \langle \mathbf{Q}_\Gamma(\Theta = 0\,\text{deg})\rangle = 3.59 \times 10^{-4}$.

If there are no other sources of rotational excitation, the angular velocity $\omega_{\text{rad}}$ gained by the grain due to the radiative torque is reached when $\mathbf{\Gamma}_{\text{rad}} = \mathbf{\Gamma}_{\text{drag,gas}}$. Thus,

$$\begin{aligned}
\omega_{\text{rad}} &= \frac{5\bar{\lambda}}{8\delta a_{\text{eff}}^2} \left(\frac{kT}{8\pi m_{\text{H}}}\right)^{1/2} \left(\frac{u_{\text{rad}}}{n_{\text{H}}kT}\right) \\
&\quad \times \left[(1 - \gamma)\langle Q_\Gamma^{\text{iso}}\rangle + \gamma\langle \mathbf{Q}_\Gamma(\Theta, \Phi)\rangle \cdot \hat{\mathbf{a}}_1\right] \left(\frac{\tau_{\text{drag}}}{\tau_{\text{drag,gas}}}\right). \tag{4.9}
\end{aligned}$$

The randomization of the rotation of the grain is caused by collisions with gas molecules. When the grain rotates much faster than the thermal rotation rate,

$$\omega_T^2 = \frac{15kT}{8\pi\alpha_1\rho a_{eff}^5}, \tag{4.10}$$

this randomization is greatly reduced. Thus, a suprathermally rotating grain is expected to be aligned with the magnetic field. The factor between the rotational rate due to the radiative torques, $\omega_{\mathrm{rad}}$, and the thermal rotational rate, $\omega_T$, is an indicator of the efficiency of the grain alignment.

$$
\begin{aligned}
\left(\frac{\omega_{\mathrm{rad}}}{\omega_T}\right)^2 &= \frac{5\alpha_1}{192\delta^2}\left(\frac{u_{\mathrm{rad}}}{n_H kT}\right)^2 \left(\frac{\rho a_{\mathrm{eff}}\bar{\lambda}^2}{m_{\mathrm{H}}}\right) \\
&\quad \times \left[(1-\gamma)\langle Q_\Gamma^{\mathrm{iso}}\rangle + \gamma\langle \mathbf{Q_\Gamma}\rangle \cdot \hat{\mathbf{a_1}}\right]^2 \left(\frac{\tau_{\mathrm{drag}}}{\tau_{\mathrm{drag,gas}}}\right)^2 \\
&= 4.72 \times 10^9 \frac{\alpha_1}{\delta^2}\rho_3 a_{-5}\left(\frac{u_{\mathrm{rad}}}{n_H kT}\right)^2 \left(\frac{\bar{\lambda}}{\mu\mathrm{m}}\right)^2 \\
&\quad \times \left[(1-\gamma)\langle Q_\Gamma^{iso}\rangle + \gamma\langle \mathbf{Q_\Gamma}\rangle \cdot \hat{\mathbf{a_1}}\right]^2 \left(\frac{\tau_{\mathrm{drag}}}{\tau_{\mathrm{drag,gas}}}\right)^2.
\end{aligned} \quad (4.11)
$$

It is worth noting here that the alignment efficiency increases rapidly with the increasing grain size.

## 4.2 Simulated polarization using radiative torques

The work presented by Draine & Weingartner (1996,1997) led to efforts to see if the predictions made by radiative torque alignment would lead to polarizations similar to those observed in dark clouds, in particular the polarization degree decreasing towards dense cloud cores (see Fig. 2.4). Cho & Lazarian (2005) made a first attempt by considering the ability of the radiative torques to align grains inside a spherically symmetric cloud. They used the radiation field inside a spherically symmetric Giant Molecular Cloud calculated by Mathis et al. (1983), and then calculated $\omega_{\mathrm{rad}}/\omega_T$ using the formalism of DW96 within the cloud. They considered only the anisotropic radiation and made the simplifying assumption that the anisotropy was along the magnetic field, and $\gamma = 0.7$. The results of Draine & Weingartner (1997) had indicated that a fast spinning grain will get aligned. Cho & Lazarian (2005) selected the criteria to be $\omega_{\mathrm{rad}}/\omega_T = 5$, and they derived a fitting formula for the minimum aligned grain size:

$$
a_{\mathrm{alg}} = (\log\ n_{\mathrm{H}})^3 (A_{\mathrm{V}} + 5)/2800\ \mu\mathrm{m}, \quad (4.12)
$$

where $A_{\mathrm{V}}$ is the visual extinction from the closest surface of the cloud. This minimum aligned grain size allowed them to calculate the Rayleigh polarization reduction factor (Greenberg, 1968; Lee & Draine 1985), which is a measure of imperfect alignment of the grain axes with respect to the magnetic field:

$$
R = \frac{\int_{a_{\mathrm{alg}}}^{a_{\mathrm{max}}} C_{\mathrm{ran}}(a)n(a)\ da}{\int_{a_{\mathrm{min}}}^{a_{\mathrm{max}}} C_{\mathrm{ran}}(a)n(a)\ da}, \quad (4.13)
$$

where $C_{\mathrm{ran}}(a)$ **is the cross section** of a randomly aligned grain, $n(a)$ the grain number density with sizes in the interval $[a, a+da]$, $a$ the grain size, $a_{\min}$ the minimum size of the grains, and $a_{\max}$ the maximum size.

Because dust is optically thin in far-infrared and sub-millimeter, the linearly-polarized components of the thermal dust emission are given by

$$q = \int R\alpha_0 \epsilon_\lambda \cos 2\psi \cos^2\gamma \, ds \, , \tag{4.14}$$

$$u = \int R\alpha_0 \epsilon_\lambda \sin 2\psi \cos^2\gamma \, ds \, , \tag{4.15}$$

where $\alpha_0$ is a coefficient of the particle properties setting the maximum polarization degree when $R = 1$, $\psi$ the angle between the projection of the magnetic field vector on the plane of the sky and the north, and $\gamma$ the angle between the local magnetic field vector and the plane of the sky. $\epsilon_\lambda$ is the dust emissivity, which is often taken to be proportional to the dust density, when not calculated with radiative transfer programs. Since we study the dust emission at FIR and sub-mm wavelengths, most of the emission comes from large grains, for which one-temperature approximation is generally used. This means that while the temperature varies from one computational cell to the next, it is a constant within the cell for all dust grains under consideration. We have only one shape for the grains, and thus $C_{\mathrm{pol}}/C_{\mathrm{ran}}$ ratio, where $C_{\mathrm{pol}}$ is the polarization cross section of the grain, is a constant, rather than depending on the size of the grain.

Cho & Lazarian (2005) presented the simulated polarization emission from a spherically symmetric cloud that they had calculated using the described method, and found that the radiative torques did produce the observed dip in the polarization degree as the dust emission intensity increased. Furthermore, the polarization degree proved to be quite sensitive to $a_{\max}$. Eq. 4.12 also showed that large grains might be aligned as deep in the cloud as $A_{\mathrm{V}} \sim 10^{\mathrm{m}}$.

Bethell et al. (2007) used a three-dimensional magnetohydrodynamic (MHD) model for a clumpy cloud. Recognizing the limitations of Cho & Lazarian (2005), they used radiative transfer modelling to derive the mean intensity and the degree of anisotropy of the radiation field in each computational cell. With this information, they calculated from Eq. 4.11 at what grain size $\omega_{\mathrm{rad}}/\omega_T = 3$, and selected that as the critical size for the aligned grains. However, they still made the simplifying assumption of unidirectional anisotropy along the magnetic field. They concluded that the patchy nature of the cloud made the mean anisotropy to be closer to 0.34 than 0.7 of the spherical cloud, but the qualitative nature of the results of Cho & Lazarian (2005) were not significantly changed.

Our studies on the efficiency of grain alignment, Papers V and VI, are summarized in Chapter 6. They are mainly based on the treatment of radiative

torques by DW96. However, Lazarian and colleagues have continued to study the theory of radiative torques.

## 4.3 Further developments of radiative torque theory

One of the problems of the radiative torque alignment is the sheer number of parameters. There are grains of different sizes, shapes and compositions, floating at different angles relative to the impinging radiation and the magnetic field. The parameter space to be explored is vast, and the calculations take a lot of time. Lazarian & Hoang (2007) introduced a simple toy model consisting of an oblate spheroid with a mirror connected to it by a thin, long and weightless rod. In their study, they demonstrated that the analytical model is able to reproduce well the results obtained for irregular grains using numerical models. In the papers that followed (e.g. Hoang & Lazarian, 2008), they have continued to use their analytical model to study the dynamics of the grain alignment by radiative torques. In their recent paper (Hoang & Lazarian, 2009), they expanded their study to more complex radiation fields, noting that in addition to unidirectional radiation fields, multipole fields should also be included to a full treatment of radiative torques. They also demonstrated the great importance of the angle between the illuminating radiation and the magnetic field, which causes an order of magnitude difference to the the radiative torque efficiency.

While the radiative torques are proving to be much more complicated than the simple treatment by DW96 allowed, the $\omega_{\mathrm{rad}}/\omega_T$ ratio continues to be a valid estimate of the radiative torque efficiency. Hence, the previous studies are not invalidated, although it needs to be recognized that the radiative torques were likely overestimated. In Paper VI, we included a case where we took into account the diminishing of the radiative torque efficiency when the magnetic field and the illuminating unidirectional radiation field were not parallel, which predictably led to weaker alignment and reduced polarization degree of the thermal dust emission.

# Chapter 5

# Summary of the publications

## 5.1 Paper I - "High-resolution mapping of interstellar clouds by near-infrared scattering"

Authors: Padoan P., Juvela M., & **Pelkonen V.-M.**

In Paper I, we propose a new method of mapping interstellar clouds by using near-IR scattered light. The intensity of the near-IR scattered light is at small optical depths linearly proportional to the column density and then saturates as the optical depth reaches $\sim 1$ in the wavelength band in question. We consider a simulated model cloud illuminated by the ISRF and compute synthetic maps of scattered light for $J$, $H$ and $K$. The true column density and the calculated intensity of scattered light are used to derive the coefficients for the analytical curve that is used to approximate the intensity as a function of the column density. We test the method by using the derived coefficients to convert the scattered light seen from a perpendicular viewing direction into a column density map. Noise has been added to the intensity to simulate an observational signal-to-noise ratio 10 at the average intensity. In the visual extinction range from 1 to 20 magnitudes, we are able to make an accurate column density map using the scattered light. Current near-IR facilities are able to reach sub-arc second spatial resolution at similar signal-to-noise ratio within reasonable exposure times. This allows the study of interstellar dust and gas structure on very small scales, almost two orders of magnitude better than what other current methods can achieve with single-dish radio or optical/NIR background star observations.

## 5.2 Paper II - "High-resolution mapping of interstellar clouds by near-infrared scattered light"

Authors: Juvela M., **Pelkonen V.-M.**, Padoan P., & Mattila, K.

In Paper II, we continue to develop the near-IR scattered light method as a tool to map large areas of interstellar clouds at high spatial resolution. We test our method on a set of model clouds provided by three-dimensional magnetohydrodynamic turbulence simulations. Radiative transfer calculations are used to derive maps of near-IR scattered light. We convert the maps of scattered light to column density with our proposed method, and compare the results with the true column densities. Background field-stars are simulated behind the same model clouds, and color excess method is used as an independent column density estimator. Real multiwavelength observations with array cameras would contain the stellar color excess information in addition to the surface brightness information, allowing us to test the two methods against one another. We study different error sources and quantify the effects that they would have on the accuracy of our estimated column density. We find that the intensity of near-IR scattered light can be used to derive a reliable estimate of the column density in regions with visual extinction less than 20 magnitudes. We find that the lower resolution information given by the color excess data is very useful in reducing the errors due to anomalous radiation field or dust properties. Even if those errors were left uncorrected, they would lead mainly to systematic "scaling" errors only, leaving the morphology of the column density map still intact. The errors can be further reduced by means of more detailed radiative transfer modelling.

## 5.3 Paper III - "A Corona Australis cloud filament seen in NIR scattered light. I. Comparison with extinction of background stars"

Authors: Juvela M., **Pelkonen V.-M.**, Padoan P., & Mattila K.

In Paper III, we present our NIR observations (NTT/SofI) of a filament in the Corona Australis molecular cloud, resulting in diffuse surface brightness maps in the $J$, $H$ and $Ks$ bands. We first test the possibility that a fraction of the surface brightness is actually thermal dust emission and not scattered light, and find no indication of significant emission even in the $Ks$ band. We show that

the scattered light can be used to accurately estimate the dust column density in the visual extinction range $A_V \approx 1$ - 15 magnitudes. We compare our results with the column density map derived from color excess method, utilizing the stars available in the observed fields. We find that the two methods agree well in regions where visual extinction is below 15 magnitudes. The existing differences are examined. Some of the differences can be explained in terms of normal observational errors. We simulate sets of synthetic star observations based on the column density map derived with color excess method. The results indicate that in the color excess method there is a bias in the interval $A_V = 15 - 20^{\mathrm{m}}$, due to the steep column density gradients that cause the small number of background stars to be sampled preferentially at low column density part within the resolution of NICER method. We conclude that the scattered light provides reliable maps of the cloud structure below $A_V \sim 15^{\mathrm{m}}$, and that the resolution is significantly better than with the color excess method.

## 5.4 Paper IV - "A Corona Australis cloud filament seen in NIR scattered light. II. Comparison of infrared and sub-millimeter data"

Authors: Juvela M., **Pelkonen V.-M.**, & Porceddu S.

In Paper IV, we expand our study of the Corona Australis molecular cloud filament to sub-millimeter range to derive the dust temperature and emissivity in the filament. The sub-mm data is provided by Spitzer 160 $\mu$m and APEX/Laboca 870 $\mu$m maps. We also extend our near-IR surface brightness observations across the filament to the south. We compare the results given by three different extinction estimators: near-IR surface brightness, color excess of background stars, and sub-mm thermal dust emission. A three-dimensional toy model, a cylinder of diameter $A_V = 10^{\mathrm{m}}$, representing the filament, and an embedded sphere of diameter $A_V = 70^{\mathrm{m}}$, representing the high column density core, provides insight on the effect of the anisotropic illumination on the near-IR surface brightness and on the reliability of the dust temperature determination. We estimate the emissivity at 870 $\mu$m to be $(1.3 \pm 0.4) \times 10^{-5}$ mag$^{-1}$, relative to the visual extinction. This is similar to the values found in diffuse medium, and a significant increase in sub-mm emissivity seems to be excluded. Near-IR surface brightness was able to pinpoint accurately the exact location of the column density maximum, even while saturated. The color excess method performed more poorly in locating the column density maximum. The near- and far-IR data agree

in indicating that the radiation field is asymmetric, the intensity being higher on the southern side of the filament. Two stars are considered to be potential additional illumination sources, and their contributions are estimated.

## 5.5 Paper V - "Simulations of polarized dust emission"

Authors: **Pelkonen V.-M.**, Juvela M., & Padoan P.

In Paper V, we test the grain alignment by radiative torques model in the case of an inhomogeneous cloud. We use the formula introduced by Cho & Lazarian (2005) (see Eq. 4.12), and apply it to a patchy cloud, whose density structure results from three-dimensional magnetohydrodynamic (MHD) simulations (see Padoan et al., 2001). While much of the model cloud volume is optically thin medium, the study concentrates on denser cores within the larger cloud, and thus the anisotropy approach by Cho & Lazarian (2005) is felt to be justified. The dust emission as well as the effective $A_V$ of each computation cell is derived using radiative transfer calculations. The effective $A_V$ is then converted to equivalent radial $A_{V,1D}$ used in the formula by Cho & Lazarian (2005). Our $P/I$-curves show quantitatively similar drop in the polarization degree towards the dense cores as the observations. The dense cores are colder than their surroundings and they emit at longer wavelengths. Thus, shorter wavelength observations see even less of the cold core. Since the polarization degree as well as the sub-millimeter emissivity is reduced in the cores, we conclude that sub-mm polarimetry carries only little information about the magnetic field within dense cores. We also make predictions concerning the polarimetric observations with the *Planck* satellite, adding noise corresponding to the sensitivity of *Planck*. We find that *Planck* is able to map polarization reliably when $A_V$ exceeds $\sim 2^m$ at spatial resolution of $\sim 15'$.

## 5.6 Paper VI - "Predictions of polarized dust emission from interstellar clouds: spatial variations in the efficiency of radiative torque alignment"

Authors: **Pelkonen V.-M.**, Juvela M., & Padoan P.

In Paper VI, we take three cores out of a larger high-resolution MHD simulation. For each core, we solve the continuum radiative transfer problem using Monte Carlo methods, which gives us the dust emission, the radiation field strength and, importantly, the direction of the incoming radiation binned in 12 discrete directions. We do a vector-sum over the directions to derive the anisotropy factor, $\gamma$, and calculate the minimum aligned grain size from Eq. 4.11 in each computational cell. We are still making the simplifying assumption of an unidirectional radiation field coming in parallel to the magnetic field. We compare our results with Paper V, and find that the slope of the $P/I$-relation is steeper, due to lower anisotropy. We show that for sightlines with $A_V$ larger than a few magnitudes, the observed polarization direction is no longer a trustworthy tracer of the mass-averaged magnetic field direction. Furthermore, we show the polarized thermal dust emission from each cell along some line of sights through the densest cores. In these cases, it is obvious that the grains are not aligned in the densest cores, and the observed polarized emission comes from the more diffuse regions in the front and behind the core. If there is grain growth in the cores, then it might be possible to reliably recover the mass-averaged magnetic field direction up to $A_V \sim 10^{\mathrm{m}}$. However, many prestellar cores may be too young for grain coagulation to play a major role. Finally, we consider a case where we take into account that the radiative torque efficiency decreases as the angle between the impinging unidirectional radiation and the magnetic field increases (see Section 4.3). This weakens the radiative torques, and even with doubled grain sizes, we are able to reliably trace the magnetic field only up to a few magnitudes of $A_V$.

## 5.7   Author's contribution to individual papers

In Paper I, the author participated in the finding of the analytical formula for the relationship between the scattered light intensities and true column densities derived from the model. He also calculated the values of the coefficients and participated in the writing of Chapter 4: Results.

In Paper II, the author was involved in the study of the analytical formula and the coefficients. He participated in the writing of Chapter 2: Conversion of near-infrared surface brightness to column density, and contributed in the interpretation of the results of the simulations.

In Paper III, the author made the observations and reduced the near-IR data used in the Paper. He wrote Chapter 2: Observations, and participated in the

writing of Chapter 4: Column densities based on scattered light. He also assisted in the interpretations of the results.

In Paper IV, the author made the additional near-IR observations used in the paper. He supervised and participated in the reduction of the near-IR data. He wrote Section 2.1: Near-infrared observations, and participated in the writing of Chapter 5: Discussion. He was involved in the interpretation of the results, and offered some suggestions as to the writing of the paper.

In Paper V, the author was responsible for the writing of the paper. P.Padoan provided the model clouds and wrote Section 3.1. M.Juvela provided the radiative transfer calculations, wrote Section 3.2 and participated in the writing of Chapter 5. The author wrote the program used to calculate the polarized thermal dust emission emerging from the clouds. The co-authors provided suggestions and corrections for the manuscript.

In Paper VI, the author was responsible for the writing of the paper. P.Padoan provided the three-dimensional model clouds. M.Juvela provided the radiative transfer code, wrote Chapter 4 and provided the spherical cloud model and the radiative transfer calculations concerning that. Both co-authors contributed to Chapter 5. The author was responsible for doing the radiative transfer calculations for the three-dimensional model clouds, and wrote the programs used to calculate the anisotropy, the efficiency of the radiative torques and the emergent polarized thermal dust emission. The co-authors provided suggestions and corrections during the writing of the paper.

# Chapter 6

# Conclusions and future prospects

The near-IR scattered light has proven to be a reliable column density estimator. The method is currently unique in combining large fields with unprecedentedly high spatial resolution. The high resolution opens up new windows in the study of interstellar dust and gas structure, down to the physical scale of the order of circumstellar disks in nearby interstellar clouds. Furthermore, the same frames that were taken for surface brightness measurements also provide stellar color excess information, allowing the two methods to be combined or checked against one another. The near-IR scattered light method carries information on the illuminating radiation field and the three-dimensional structure of the cloud. These qualities make it an very versatile tool in studying the interstellar clouds.

We have continued our work by observing other clouds in addition to the Corona Australis filament. A larger sample allows us to test our method in different environments and cloud structures. An open question still remains if dust emission could cause a small excess to the $Ks$-band surface brightness. While no such indication was seen in the Corona Australis filament, we are currently reducing data on other clouds obtained by UKIRT/WFCAM and NTT/SofI. In addition, we have *AKARI* observations on CG31 in Gum Nebula, straddling the wavelength range beyond the $Ks$-band where the dust emission should become the dominant contributor to the surface brightness. Detection would give us a point which we could extrapolate down to $Ks$-band, while a non-detection of the dust emission would give us a valuable upper limit.

The other topic of this thesis is the polarized thermal dust emission and particularly the grain alignment by radiative torques. Thanks to the quantitative treatment of radiative torques starting from Lazarian & Hoang (2007), the theory is reaching a mature stage where predictions about the alignment of the grains and the arising polarization are possible. The results of Paper VI imply that the Chandrasekhar-Fermi method may not be reliable when trying to derive the magnetic field inside dense cores. We intend to study this question in our future

papers.

New observational data is coming; *Planck* Satellite was launched in May 2009, and it will perform all-sky polarization measurements from 353 GHz to 30 GHz. Studies such as Papers V and VI will be necessary in interpreting the observations made by *Planck* and in removing the foreground dust component from the cosmic microwave background. SCUBA-2, installed at James Clark Maxwell Telescope in Hawaii, will offer polarized dust emission observations at 450 and 850 $\mu$m. The spatial resolution of SCUBA-2 is much better than that of *Planck*, 14 arc seconds vs. 5 arc minutes at 850 $\mu$m. Once SCUBA-2 becomes operational, estimated to happen during 2009, it will be capable of producing high resolution maps of the polarized thermal dust emission from interstellar clouds.

# References

[1] Adams W.S., 1949, ApJ, 109, 354

[2] Anderson C.M., Weitenbeck A.J., Code A.D., Nordsieck K.H, Meade M.R., et al., 1996, AJ, 112, 2726

[3] Aschenbach B., 1988, in *Supernova Remnants and the Interstellar Medium*, IAU Symposium No. 101, edited by R.S. Roger and T.L. Landecker (Cambridge University, Cambridge), p. 99

[4] de Avillez M.A., & Breitschwerdt D., 2004, A&A, 425, 899

[5] Barnard E., 1927, in A Photographical Atlas of Selected Regions of the Milky Way, edited by E. Frost & M. Calvert (Washington DC, Carnegie Institute)

[6] Beals C.S., 1936, MNRAS, 96, 661

[7] Bernard J.-P., Abergel A., Ristorcelli I., Pajot, F., Torre, J.P., et al., 1999, A&A, 347, 640

[8] Bethell T.J., Chepurnov A., Lazarian A., & Kim J., 2007, ApJ, 663, 1055

[9] Blandford R.D., & Eichler D., 1987, Phys. Rep., 154, 1

[10] Bloemen H., 1987, in *Interstellar Processes*, edited by D.J. Hollenbach and H.A. Thronson, Jr. (Reidel, Dordrecht), p. 143

[11] Bohlin R.C., 1975, ApJ, 200, 402

[12] Bohlin R.C., Savage B.D., & Drake J.F., 1978, ApJ, 224, 132

[13] Bothe W., & Kohlhörster W., 1929, Z.Phys., 56, 751

[14] Boudet N., Mutschke H., Nayral C., et al., 2005, ApJ, 633, 272

[15] Boulanger F., Abergel A., Bernard J.-P., Burton W.B., Desert F.-X., et al., 1996, A&A, 312, 256

[16] Boulanger F., & Perault M., 1988, ApJ, 330, 964

[17] Cambresy L., Beichman C.A., Jarrett T.H., & Cutri R.M., 2002, AJ, 123, 2559

[18] Cambresy L., Boulanger F., Lagache G., & Stepnik, B., 2001, A&A, 375, 999

[19] Cardelli J.A., Clayton G.C, Mathis J.S, 1989, ApJ, 345, 245

[20] Carruthers G., 1970, ApJL, 161, L81

[21] Chandrasekhar S., & Fermi E., 1953, ApJ, 118, 113

[22] Cho J., & Lazarian A., 2005, ApJ, 631, 361

[23] Clayton G.C., & Mathis J.S., 1988, ApJ, 327, 911

[24] Clayton G.C., Wolff M.J., Allen R.G., Lupie O.L., 1996, ApJ, 445, 947

[25] Clemens D.P., Sanders D.B., & Scoville N.Z., 1988, ApJ, 327, 139

[26] Cox D.P., & Smith B.W., 1974, ApJL, 189, L105

[27] Crutcher R.M., 1999, ApJ, 520, 706

[28] Dame T.M., Hartmann D., & Thaddeus P., 2001, ApJ, 547, 792

[29] Davis L., & Greenstein J.L., 1951, ApJ, 114, 206

[30] Desert F.-X., Boulanger F., & Puget J.-L., 2008, A&A, 237, 215

[31] Desert F.-X., Macias-Perez J.F., Mayet F., Giardino G., Renault C., et al., 2008, A&A, 481, 411

[32] Dickinson C., Davies R.D., & Davis R.J., 2003, MNRAS, 341, 369

[33] Dickley J.M, Terzian Y., & Salpeter E.E., 1978, ApJSS, 36, 77

[34] Dolginov A.Z., 1972, Ap&SS, 18, 337

[35] Dolginov A.Z., & Mytrophanov I.G., 1976, Ap&SS, 43, 291

[36] Domgörgen H., & Mathis J.S., 1994, ApJ, 428, 647

[37] Dove J.B., & Shull J.M., 1994, ApJ, 430, 222

[38] Dove J.B., Shull J.M., & Ferrara A., 2000, ApJ, 531, 846

[39] Draine B.T., 2003a, ARA&A, 41, 241

[40] Draine B.T., 2003b, ApJ, 598, 1017

[41] Draine B.T., & Flatau P., 1994, JOSAA, 11, 1491

[42] Draine B.T., & Lee H.M., 1984, ApJ, 285, 89

[43] Draine B.T., & Li A., 2001, ApJ, 551, 807

[44] Draine B.T., & Weingartner J., 1996, ApJ, 470, 551

[1997] Draine B.T., & Weingartner J., 1997, ApJ, 480, 633

[45] Duley W.W., & Williams D.A., 1981, MNRAS, 196, 269

[46] Dupac X., Bernard J.-P., Boudet N., et al., 2003, A&A, 404, L11

[47] Dwek, E., Arendt R.G, Fixsen D.J, Sodroski T.J., Odegard, N., et al., 1997, ApJ, 475, 565

[48] Elvey C.T., & Roach F.E., 1937, ApJ, 85, 213

[49] Ewen H.I., & Purcell E.M., 1951, Nature (London), 168, 356

[50] Falceta-Goncalves D., Lazarian A., & Kowal G., 2008, ApJ, 679, 537

[51] Falgarone E., Troland T.H., Crutcher R.M., & Paubert G., 2008, A&A, 487, 247

[52] Ferriere K.M., 1998, ApJ, 503, 700

[53] Ferriere K.M., 2001, ARA&A, 73, 1031

[54] Field G.B., Goldsmith D.W., & Habing H.J., 1969, ApJL, 155, L149

[55] Fitzpatrick E.L., 1999, PASP, 111, 63

[56] Foster J., & Goodman A., 2006, ApJ, 636, L105

[57] Gerakines P.A., Whittet D.C.B., & Lazarian A., 1995, ApJ, 455, L171

[58] Gilra D.P., 1972, in *Scientific Results from the Orbitting Astronomical Observatory OAO-2*, NASA SP-310, edited by A.D. Code (National Aeronautics and Space Administration, Washington, D.C.), p. 295

[59] Ginzburg V.L., & Syrovatskii S.I., 1965, ARA&A, 3, 297

[60] Goldsmith D.W., 1987, in *Interstellar Processes*, edited by D.J. Hollenbach and H.A. Thronson, Jr. (Reidel, Dordrecht), p. 51

[61] Goldsmith D.W., Habing H.J., & Field G.B., 1969, ApJ, 158, 173

[62]  Goodman A.A., Jones T.J., Lada E.A., & Myers P.C., 1992, ApJ, 399, 108

[63]  Goodman A.A., Jones T.J., Lada E.A., & Myers P.C., 1995, ApJ, 448, 748

[64]  Greenberg J.M., 1968, in *Nebulae and Interstellar Matter*, Vol. 7, edited by G.P. Kuiper and B.M. Middlehurst (University of Chicago Press, Chicago), p. 328

[65]  Grabelsky D.A., Cohen R.S., Bronfman L., & Thaddeus P., 1987, ApJ, 315, 122

[66]  Haffner L.M., Reynolds R.J., Tufte S.L., Madsen G.J., Jaehnig K.P., & Percival J.W., 2003, ApJSS, 149, 405

[67]  Haikala L.K., Mattila K., Bowyer S., et al., 1995, ApJ, 443, L33

[68]  Hall J.S., 1949, Science, 109, 166

[69]  Hartmann J., 1904, ApJ, 19, 268

[70]  Haslam C.G.T., Salter C.J., Stoffel H., & Wilson W.E., 1982, A&AS, 47, 1

[71]  Heiles C., 1987, ApJ, 315, 555

[72]  Heiles C., 1990, ApJ, 354, 483

[73]  Heiles C., 2000, AJ, 119, 923

[74]  Heitsch F., Zweibel E., Mac Low M.M., Li P.S., & Norman M.L., 2001, ApJ, 561, 800

[75]  Henyey L.G., & Greenstein J.L., 1941, ApJ, 93, 70

[76]  Henning T., Wolf S., Launhardt R., & Walters R., 2001, ApJ, 561, 871

[77]  Hess V., 1919, Phys.Z., 13, 1048

[78]  Heyer M.H., 1999, in *New Perspectives on the Interstellar Medium*, Astronomical Society of the Pacific Conference Series Vol. 168, edited by A.R. Taylor, T.L. Landecker and G. Joncas (ASP, San Francisco), p. 55

[79]  Heyer M.H., Brunt C., Snell R.L, Howe J.E., Schloerb F.P., & Carpenter J.M., 1998, ApJSS, 115, 241

[80]  Hildebrand R.H., Dotson J.L., Dowell C.D., Schleuning D.A., & Vaillancourt J.E., 1999, ApJ, 516, 834

[81]  Hiltner W., 1949, Science, 109, 166

[82] Hoang T., & Lazarian A., 2008, MNRAS, 388, 117

[83] Hoang T., & Lazarian A., 2009, ApJ, 697, 1316

[84] Jenkins E.B., 1987, in *Interstellar Processes*, edited by D.J. Hollenbach and H.A. Thronson, Jr. (Reidel, Dordrecht), p. 533

[85] Jenkins E.B., & Meloy D.A., 1974, ApJL, 193, L121

[86] Jenkins E.B., & Savage B.D., 1974, ApJ, 187, 243

[87] Juvela M., Mattila K., Lehtinen K., Lemke D., Laureijs R., & Prusti T., 2002, A&A, 382, 583

[88] Kainulainen J., Lehtinen K., & Harju J., 2006, A&A, 447, 597

[89] Kim S.-H., & Martin P.G., 1995, ApJ, 444, 293

[90] Knacke R.F., & Thomson R.K., 1973, PASP, 85, 341

[91] Korpi M.J., Brandenburg A., Shukurov A., Tuominen I., & Nordlund Å., 1999, ApJL, 514, L99

[92] Kulkarni S.R., Blitz L., & Heiles C., 1982, ApJL, 259, L63

[93] Kulkarni S.R., & Heiles C., 1987, in *Interstellar Processes*, edited by D.J. Hollenbach and H.A. Thronson, Jr. (Reidel, Dordrecht), p. 87

[94] Lada C.J., Lada E.A., Clemens D.P., & Bally J., 1994, ApJ, 429, 694

[95] Lagache G., Abergel A., Boulanger F., & Puget J.-L., 1998, A&A, 333, 709

[96] Lagache G., Haffner L.M., Reynolds R.J., & Tufte S.L., 2000, A&A, 354, 247

[97] Lai S.P., Crutcher R.M., Girart J.M., & Rao R., 2001, ApJ, 561, 864

[98] Larson R.B., 1981, MNRAS, 194, 809

[99] Lazarian A., 2007, JQSRT, 106, 225

[100] Lazarian A., & Hoang T., 2007, MNRAS, 378, 910

[101] Lee H., & Draine B.T., 1985, ApJ, 290, 211

[102] Leger A., & Puget J.-L., 1984, A&A, 137, L5

[103] Lehtinen K., & Mattila K., 1996, A&A, 309, 570

[104]  Lehtinen K., Mattila K., Lemke D., Juvela M., Prusti T., & Laureijs R., 2003, A&A, 398, 571

[105]  Li A., & Draine B.T., 2001, ApJ, 554, 778

[106]  Lombardi M., 2005, A&A, 438, 169

[107]  Lombardi M., 2009, A&A, 493, 735

[108]  Lombardi M., & Alves J., 2001, A&A, 377, 1023

[109]  Lombardi M., Alves J., & Lada C.J., 2006, A&A, 454, 781

[110]  Lombardi M., Lada C.J., & Alves J., 2008, A&A, 480, 785

[111]  Mallik D.C.V., 1975, ApJ, 197, 355 ; 200, 803(E)

[112]  Maloney P., 1990, ApJL, 348, L9

[113]  Mathewson D.S., & Ford V.L., 1970, Mem.R.Astron.Soc., 74, 139

[114]  Mathis J.S., 1986, ApJ, 301, 423

[115]  Mathis J.S., 1987, in *Exploring the Universe with the IUE Satellite*, edited by Y. Kondo and W. Wamsterker (Kluwer, Dordrecht), p. 517

[116]  Mathis J.S., Mezger P.G., & Panagia N., 1983, A&A, 128, 212

[117]  Mathis J.S., Rumpl W., & Nordsieck K.H., 1977, ApJ, 217, 425

[118]  Mattila K., 1970a, A&A, 8, 273

[119]  Mattila K., 1970b, A&A, 9, 53

[120]  McCammon D., & Sanders W.T., 1990, ARA&A, 28, 657

[121]  McCarthy J.F., Forrest W.J, Briotta D.A., & Houck J.R., 1980, ApJ, 242, 965

[122]  McCray R., & Snow T.P., Jr., 1979, ARA&A, 17, 213

[123]  McKee C.F., 1990, in *The Evolution of the Interstellar Medium*, Astronomical Society of the Pacific Conference Series Vol. 12, edited by L. Blitz (ASP, San Francisco), p. 55

[124]  McKee C.F., & Ostriker J.P., 1977, ApJ, 218, 148

[125]  Menella V., Brucato J.R., Colangeli L., et al., 1998, ApJ, 496, 1058

[126] Merrill P.W., 1934, PASP, 46, 206

[127] Mestel L., 1985, in *Protostars and Planets II*, edited by D.C. Black and M.S. Matthews (University of Arizona, Tucson), p. 320

[128] Mihalas D. & Binney J., 1981, in *Galactic Astronomy: Structure and Kinematics* (Freeman, San Francisco)

[129] Miller W.W., & Cox D.P., 1993, ApJ, 417, 579

[130] Miville-Deschênes M.-A., & Lagache G., 2005, ApJS, 157, 302

[131] Morton D.C., 1967, ApJ, 147, 1017

[132] Myers P.C., 1987, in *Interstellar Processes*, edited by D.J. Hollenbach and H.A. Thronson, Jr. (Reidel, Dordrecht), p. 71

[133] Myers P.C., Goodman A.A., Gusten R., & Heiles C., 1995, ApJ, 442, 177

[134] Nakajima Y., Kandori R., Tamura M., et al., 2008, PASJ, 60, 731

[135] Nakajima Y., Nagata T., Sato S., et al., 2003, AJ, 125, 1407

[136] Nakano T., 1979, PASJ, 31, 697

[137] Odegard N., Arendt R.G., Dwek E., Haffner L.M., Hauser M.G., & Reynolds R.J., 2007, ApJ, 667, 11

[138] Oort J.H., Kerr F.J., & Westerhout G., 1958, MNRAS, 118, 379

[139] Ossenkopf V., & Henning T., 1994, A&A, 291, 943

[140] Osterbrock D.E., 1989, *Astrophysics of Gaseous Nebulae and Active Galactic Nuclei* (University science Books, Mill Valley, CA)

[141] Ostriker E.C., Stone J.M., & Gammie C.F., 2001, ApJ, 546, 980

[142] Padoan P., Bally J., Billawala Y., Juvela M., & Nordlund Å., 1999, ApJ, 525, 318

[143] Padoan P., Goodman A., Draine B.T., Juvela M., Nordlund Å., & Rognvaldsson Ö.E., 2001, ApJ, 559, 1005

[144] Pagani L., Lagache G., Bacmann A., et al., 2003, A&A, 406, L59

[145] Purcell E.M., 1975, in *The Dusty Universe*, edited by G.B. Field & A.G.W. Cameron (Neal Watson, New York), p. 155

[146] Rand R.J., & Kulkarni S.R., 1989, ApJ, 343, 760

[147]  Reynolds R.J., 1984, ApJ, 282, 191

[148]  Reynolds R.J., 1985, ApJ, 294, 256

[149]  Reynolds R.J., Haffner L.M., & Tufte S.L, 1999, ApJL, 525, L21

[150]  Ridderstad M., Juvela M., Lehtinen K., Lemke D., & Liljeström T., 2006, A&A, 451, 961

[151]  Ristorcelli I., Serra G., Lamarre J.-M., Giard M., Pajot F., et al, 1998, ApJ, 496, 267

[152]  Roesler F.L., Reynolds R.J., Schreb F., & Ogden P.M., 1978, in *High Resolution Spectroscopy*, Proceedings of the Fourth Colloquium on Astrophysics of the Trieste Observatory, edited by M. Hack (Osservatorio Atronomico di Trieste, Trieste), p. 600

[153]  Russell H.N., 1935, MNRAS, 95, 610

[154]  Savage B.D., & Jenkins E.B., 1972, ApJ, 172, 491

[155]  Savage B.D., & Mathis J.S., 1979, ARA&A, 17, 73

[156]  Scheffler H., & Elsässer H., 1988, in *Physics of the Galaxy and interstellar matter* (Springer-Verlag, Berlin-Heidelberg), p. 420

[157]  Schlegel D.J., Finkbeiner D.P., & Davis M., 1998, ApJ, 500, 525

[158]  Scoville N.Z., & Saunders D.B., 1987, in *Interstellar Processes*, edited by D.J. Hollenbach and H.A. Thronson, Jr. (Reidel, Dordrecht), p. 21

[159]  Serkowski K., 1973, in *Interstellar Dust and Related Topics*, IAU Symposium No. 52, edited by J.M. Greenberg, H.c. van de Hulst (Reidel, Dordrecht), p. 145

[160]  Shu F.H., Adams F.C., & Lizano S., 1987, ARA&A, 25, 23

[161]  Sivan J.-P., 1974, A&ASS, 16, 163

[162]  Sivan J.-P., Stasinska G., & Lequeux J., 1986, A&A, 158, 279

[163]  Slavin J.D., & Cox D.P., 1993, ApJ, 417, 187

[164]  Smith A.M., & Stecher T.P., 1971, ApJL, 164, L43

[165]  Smith C.H., Wright C.M., Aitken D.K., Roche P.F. & Hough J.H., 2000, MNRAS, 312, 327

[166] Snowden S.L., Egger R., Finkbeiner D.P., Freyberg M.J., & Plucinsky P.P., 1998, ApJ, 493, 715

[167] Spitzer L., Jr., 1956, ApJ, 124, 20

[168] Spitzer L., Jr., 1958, in *Electromagnetic Phenomena in Cosmical Physics*, IAU Symposium No. 6, edited by B. Lehnert (Cambridge University, Cambridge), p. 169

[169] Spitzer L., Jr., 1990, ARA&A, 28, 71

[170] Stecher T.P., 1965, ApJ, 142, 1683

[171] Stecher T.P., & Donn B., 1965, ApJ, 142, 1681

[172] Struve O., 1937, ApJ, 86, 94

[173] Struve O., & Elvey C.T., 1936, ApJ, 83, 167

[174] Struve O., & Elvey C.T., 1938, ApJ, 88, 364

[175] Swings P., & Rosenfeld L., 1937, ApJ, 86, 483

[176] Troland T.H., & Crutcher R.M., 2008, ApJ, 680, 457

[177] Troland T.H., & Heiles C., 1986, ApJ, 301, 339

[178] Trumpler R.J., 1930, PASP, 42, 214

[179] van de Hulst H. C., 1945, Nederlands Tijdschrift voor Natuurkunde, 11, 201

[180] Van Steenberg M.E., & Shull J.M., 1988, ApJ, 330, 942

[181] Vershuur G.L., 1969, ApJ, 156, 861

[182] Ward-Thompson D., Kirk J.M., Crutcher R.M., Greaves J.S., Holland W.S., & Andre P., 2000, ApJL, 537, L135

[183] Webber W.R., 1983, in *Composition and Origin of Cosmic Rays*, edited by M.M. Shapiro (Reidel, Dordrecht), p. 83

[184] Weingartner J.C., & Draine B.T., 2001, ApJ, 547, 296

[185] Welty D.E., & Fowler J.R., 1992, ApJ, 393, 193

[186] Whittet D.C.B., Bode M.F., Longmore A.J., et al., 1988, MNRAS, 233, 321

[187] Whittet D.C.B., Hough J.H., Lazarian A., & Hoang T., 2008, ApJ, 674, 304

[188] Wilking B.A., Lebofsky M.J., & Rieke G.H., 1982, AJ, 87, 695

[189] Williamson F.O., Sanders W.T., Kraushaar W.L., McCammon D., Borken R., & Bunner A.N., 1974, ApJL, 193, L133

[190] Wilson R.W., Jefferts K.B., & Penzias A.A., 1970, ApJL, 161, L43

[191] Witt A.N., 1968, ApJ, 152, 59

[192] Wolf M., 1923, AN, 219, 109

[193] Wolff M.J., Clayton G.C., Kim S.H., Martin P.G., & Anderson C.M., 1997, ApJ, 479, 395

[194] York D.G., 1974, ApJL, 193, L127

[195] York D.G., 1977, ApJ, 213, 43

# Journal abbreviations

| | |
|---|---|
| A&A | Astronomy & Astrophysics |
| A&ASS | Astronomy & Astrophysics Supplement |
| AJ | The Astronomical Journal |
| AN | Astronomische Nachrichten |
| ApJ | The Astrophysical Journal |
| ApJL | The Astrophysical Journal Letters |
| ApJSS | The Astrophysical Journal Supplement Series |
| Ap&SS | Astrophysics and Space Science |
| ARA&A | Annual Review of Astronomy & Astrophysics |
| JOSAA | Journal of the Optical Society of America A |
| JQSRT | Journal of Quantitative Spectroscopy and Radiative Transfer |
| Mem.R.Astron.Soc. | Memoirs of the Royal Astronomical Society |
| MNRAS | The Monthly Notices of the Royal Astronomical Society |
| Nature | Nature |
| PASP | Publications of the Astronomical Society of the Pacific |
| PASP | Publications of the Astronomical Society of Japan |
| Phys. Rep. | Physics Reports |
| Phys.Z. | Physikalische Zeitschrift |
| Science | Science |
| Z.Phys. | Zeitschrift für Physik |